Lawrence Berkeley Laboratory

UNIVERSITY OF CALIFORNIA

Materials & Chemical Sciences Division

Nb Modification of Microcomposite Fe/C/Cr/Mn Steel

J. Kim
(Ph.D. Thesis)

December 1988

Prepared for the U.S. Department of Energy under Contract Number DE-AC03-76SF00098.

DISCLAIMER

LBL-26145

Nb Modification of Microcomposite Fe/C/Cr/Mn Steel

Jongkeun Kim
(Ph.D. Thesis)

Department of Materials Science and Mineral Engineering
University of California
and
Materials and Chemical Sciences Division
Lawrence Berkeley Laboratory
1 Cyclotron Road
Berkeley, California 94720
USA

December 1988

Nb MODIFICATION OF MICROCOMPOSITE Fe/C/Cr/Mn STEEL

Jongkeun Kim

Ph.D.

Sponsor: Pohang Iron and Steel Co., Korea
U. S. Department of Energy

ABSTRACT

A microcomposite steel which is desired to be attained in this investigation, is a composite microstructure consisting of fine packets of heavily dislocated martensite laths surrounded by continuous thin films of interlath retained austenite. Heavily dislocated lath martensite gives ultrahigh strength; a softer, tough austenite phase provides high fracture toughness. This composite microstructure has been achieved in the Fe/Cr/Mn/C system containing more than a total of four percent of alloying elements in previous work.

The present work is concerned with obtaining superior combinations of mechanical properties by adding the microalloy element of niobium to the basic quaternary alloy of Fe/2.0 wt% Cr/1.2 wt% Mn/0.25 wt% C and by applying controlled rolling

practice to processing of the experimental alloys to attain fine austenite grains, giving rise to high Charpy V-notch impact toughness. The basis is to have sufficient hardenability after retrenching the chromium content, so that processing will not destroy the microcomposite structure of heavily dislocated martensite laths and thin films of interlath retained austenite after the martensitic phase transformation, following rolling and quenching.

Continuous cooling transformation diagrams of the basic quaternary and the niobium bearing alloys have been determined to predict the appropriate cooling rate required for martensitic transformation by dilatometry method. Niobium effected a considerable increment of martensitic hardenability, which alleviates the otherwise stringent quenching rate arising from the reduced alloy contents and which is needed to obtain the composite microstructure.

Controlled rolling practice has been widely utilized commercially for refining ferrite grain size in ferrite/pearlite steels, by applying heavy deformation below the recrystallization temperature, in order to obtain the pancake structure of austenite. However, in this work, heavy deformation is added just above the recrystallization temperature in order to obtain fine and recrystallized austenite grains which result in fine microcomposite structures. Thus the rolling conditions (amount of deformation, temperature) were optimised in this study. As for the microalloy element, 0.02 wt% of niobium is added to utilize

the interactions of microalloyed element precipitation and austenite recrystallization kinetics during hot rolling. Application of controlled rolling practice to Fe/0.25 wt% C/2.0 wt% Cr/1.2 wt% Mn/0.02 wt% Nb alloy resulted in a great enhancement of Charpy impact toughness by about 15 joules than Fe/0.25 wt% C/2.0 wt% Cr/1.2 wt% Mn alloy without addition of niobium.

Plane strain fracture toughness tests were done on both experimental alloys which were treated with optimum process condition. This condition involves finish rolling at 900°C followed by water quenching and tempering at 250°C. The Nb bearing alloy showed an excellent plane strain fracture toughness value reaching 155 MPa$\sqrt{m}$, after tempering but even 147 MPa$\sqrt{m}$ directly quenched on-line. These good values are due to the composite structure.

Table of Contents

1. Introduction

Ultrahigh strength steels have wide applications such as aircraft undercarriages, high strength bolts and fasteners, rocket motor cases, missile bodies, springs, high-speed rotors, bearings and shafts. The impetus for their development arose from aerospace and aircraft requirements initially, in response to the development of the highest strength aluminium alloys which, however, could not match steels with respect to elastic modulus and impact resistance. The major requirements for this type of steel are strength, toughness, ductility, fatigue strength and weldability (1).

Among these requirements, strength, toughness, and ductility are undoubtedly the most important properties specified for ultrahigh strengh steels. The major difficulty in optimising these properties comes from the fact that strength is usually inversely related to toughness and ductiliy; the increase in the former is achieved at the expense of the latter and vice versa. Conventional manipulation of mechanical properties through microstructural control has shown that high strength and high toughness are often conflicting requirements, as an increase in strength is often accompanied by a reduction in the ductility and fracture toughness. Typical microstructural effects that show this trend are solute strengthening, precipitation hardening and dislocation hardening. Nevertheless, two methods of microstructural control are available that result in an increase

in both properties: grain refinement and phase transformation through heat treatment. The principles of composites (viz. mixing hard and ductile but tough phases with coherent interfaces) have formed the basis for alloy design programs that have been developed at U. C. Berkeley (2).

As a continuing program on alloy design, the principles of microcomposite structure are utilized to achieve superior combinations of mechanical properties, e.g., strength and toughness. In the particular class of HSLA steels dealt with here, the microcomposite consists of fine grained heavily dislocated packet lath martensite in which the laths are surrounded by thin films of retained austenite as shown in Fig. 1. The dislocations are a necessary component for both strength and toughness. Whether twinned or dislocated slip martensite occurs is determined mainly by the composition of the steel, in particular, the carbon content through its effect on the martensitic transformation start temperature.

A significant observation made recently using careful methods of transmission electron microscopy is the identification of thin interlath films of retained austenite. Since this discovery, several investigators (3-8) attributed improved fracture toughness properties to the presence of this form of retained austenite. Although in some instances the improvement in toughness properties could not be singly attributed to the retained austenite, best properties were always associated with microstructures containing large quantities of stable retained

austenite. Plane strain fracture toughness has been greatly enchanced by the thin films of retained austenite which are capable of blunting moving cracks or causing them to branch out and thus increase stress necessary for further movement of cracks. These structures have been obtained by developing Fe/C/Cr/Mn compositions maintaining M_S>300°C to avoid twinning as well as to obtain autotempering on cooling.

Carbon is by far the most effective and economical way of raising the strength of steel (9). While significant gains in strength could be obtained through carbon additions, the toughness deteriorates monotonically. From a fracture mechanics viewpoint, increasing strength without a corresponding increase in toughness would only result in poor utilization of the available strength of steel in engineering applications where resistance to the propagation of existing cracks is important. Above 0.35 wt% C, martensitic steel attains significant contribution to strengthening from substructural twinning. However, this kind of strengthening is undesirable from a toughness viewpoint. Thus, with a view to designing tough structural steels at a tensile strength level of 1400 MPa, the carbon content of the experimental alloys used in this investigation is selected as 0.25 wt%.

Chromium has been selected as a ternary element after the observation of Thomas and McMahon (10) that Fe/C/Cr experimental alloys produce a microcomposite structure of fine packets of martensite laths and thin films of retained austenite,

which gives a beneficial effect on fracture toughness. In general, chromium has several other effects: (1) solid solution hardening, (2) depression of M_S temperature and corrosion improvement, and (3) retardation of the tempering process. Chromium content has been reduced to 2 wt% in this investigation.

Manganese increases hardenability of experimental alloys substantially. Nevertheless, excessive additions of manganese are to be avoided, for it was shown that in medium carbon steels, manganese leads to large fractions of twinned substructures and secondly, since manganese lowers M_S temperature significantly, higher manganese contents result in the suppression of autotempering and severe quench cracking. It is reported that manganese addition lowers DBTT (11). Manganese is also a fcc stabilizer which would promote retention of austenite in the as-quenched structures of midium carbon steels. Manganese composition was decided at 1.2 wt%.

Niobium , the most important microalloying element, adjusts the structural parameters of the product, e.g. prior austenite grain size, through controlling the basic processes of recrystallization and precipitation, and transformation kinetics (12). However, its content is limited by the temperature dependent solubility product relationship. With 0.02 wt% of niobium added to the basic quaternary alloy, the microcomposite microalloying principle was employed to obtain fine recrystallized austenite grains wnich results in fine packets of

martensite laths and retained austenite. The comparison of principles between conventional microalloying and microcomposite microalloying is shown in Fig. 2. The effect of the niobium was investigated by comparing the mechanical properties and microstructures of the basic quaternary alloy with the niobium bearing alloy.

Perhaps the microstructural feature which influences, more than any other, the properties and reponse of metals to heat treatment, is the prior austenite grain size (13-15). It influences not only the yield and tensile strengths, but also the tensile ductility, Charpy toughness and ductile-brittle transition temperature. Also, the austenite grain size affects the transformation characteristics of a steel. It is, therefore, no exaggeration to state that control over the grain size enables the whole response of steels to heat treatment, and the subsequent mechanical properties, to be influenced. It is not surprising, therefore, that much time and effort have been devoted to investigation of methods which can be used to control the grain size of steels. These have been developed to a fairly high degree of commercial reproducibility. Therefore, understanding of the processes controlling the grain size is important in processing of steel. However, sufficiently high austenitizing solution temperatures are needed to ensure all carbides etc. are initially in solid solution. Subsequent processing then must refine the grain size. In this work a solution temperature of 1200°C was necessary.

The austenite grain size can be reduced by means of retardation of grain boundary migration by microalloy element solutes and precipitated particles. In addition to the microalloy element composition, the processing parameters play an important role in obtaining an achievable grain refinement. It is characterized by particularly great effects produced at relatively low concentrations. This is due to the very fine dispersion of precipitates forming in the austenite. These precipitates are high-carbon carbonitrides of the Nb(C,N) type in which the percentage of carbon and nitrogen is governed by the basic composition and the precipitation temperature. Deformation within the lower austenite temperature range leads to strain induced precipitation of finely dispersed carbonitrides which cause retardation of recrystallization and grown growth (16).

In order to obtain fine grained austenite, which results in fine microcomposite structure, a clear understanding of the recrystallization kinetics of austenite during hot deformation, and precipitation kinetics of the microalloy element carbonitrides and their interaction with recrystallization kinetics is important in processing the experimental alloys.

During deformation at strain rates and temperatures of interest in hot working operations, all metals undergo work hardening and dynamic recovery and some may also undergo dynamic recrystallization. The microstructures produced by these processes are unstable and, on holding at temperature

after the end of deformation, further structural changes occur by static recovery, recrystallization, and grain growth. In hot rolling operations, dynamic and static structural changes that take place during and between passes interact to determine the overall evolution of microstructure (17).

During hot deformation of steels in the austenitic condition, the flow stress initially rises with strain as a result of work hardening and recovery; dislocation density rises and subgrain structure tends to develop. Because dynamic recovery is relatively slow, the subgrain boundaries are ill formed, and sufficient strain energy is stored to nucleate dynamic recrystallization when a critical strain is reached. This provides an additional softening mechanism and results in a fall in flow stress until a steady-state level is reached after a strain interval in which a large fraction of recrystallization has taken place. The dynamic softening processes are thermally activated, giving a dependence of stress on strain rate $\dot{\varepsilon}$ and temperature T, which, in case of C-Mn steel, can be described in terms of the Zener-Hollomon parameter Z as

$$Z = \dot{\varepsilon} \exp Q/RT \qquad (1)$$

over the range of conditions of interest in hot rolling. Here $\dot{\varepsilon}$ is the strain rate, Q is a activation energy for self diffusion of iron, R is gas constant, and T is absolute temperature.

Static recrystallization accompanyied by hot deformation

proceeds in a similar manner to that in cold worked material. Nucleation sites for new grains are predominantly triple junctions of grains and grain boundaries. The distribution of nuclei is highly localized and inhomogeneous; while some grain boundaries give rise to numerous nuclei, there are boundaries where nuclei are completely absent. The progress of recrystallization after nucleation is essentially the migration of recrystallizing front into deformed matrix as is usual in recrystallization. The completion of recrystallization is followed by normal grain growth.

The recrystallized grain size decreases rapidly as the amount of reduction increases, reaching a limiting value. The limiting grain size decreases with reducing initial grain size. Although a lower deformation temperature produces smaller grain sizes, the effect of temperature is slight. Since nucleation sites for recrystallization are predominantly at the grain boundaries, the initial grain size plays an important role in determining recrystallized grain size (18).

However, it must be emphasized that static recrystallization accompanyied by hot deformation does not occur under all conditions. It is necessary to apply more deformation than that required for recrystallization. The critical amount of deformation required for the completion of recrystallization is small, as is the temperature dependence in plain carbon steel. In niobium steel, it is very large and its temperature dependence is substantially higher (19).

When recrystallization is complete, further grain growth takes place to reduce the grain boundary area per unit volume. Grain growth is a thermally activated process, and the grain size which is developed depends both on time and temperature. Other factors, however, are known to influence the migration of grain boundaries. These include the concentration of solute elements and second phase particles at grain boundaries, which can introduce a frictional drag on the moving boundary, and which decrease the grain-boundary area, and hence the overall grain-boundary energy.

Some attempts have been made to develop a satisfactory theory for the effects of precipitate particles on austenite grain growth. Zener considered the relationship between the size of spherical grains, of radius R, and the radius of associated spherical precipitate particles, r. Zener's criterion was:

$$R = 4\,r / 3\,f \qquad (2)$$

where f is the volume fraction of precipitate particles. This may be expected to overestimate the driving force for grain growth, because it is derived from a model of an isolated contracting spherical grain (20). In fact, the substitution of typical precipitate particle sizes and volume fractions into the Zener equation indicates a much larger equilibrium grain size than is observed. This observation confirms that the driving force for grain growth is overestimated in the Zener model.

The influence of the precipitation process on recrystallization and grain growth in microalloyed steels has

been the subject of numerous studies. In general, fine particles (≈ 6 nm dia) deposited on dislocations, even when present in very small volume fractions (≈ 0.03 %), can retard recrystallization and grain growth significantly, while coarser precipitates (> 20 nm dia.) have less effect (21).

The retarding effect due to the strain induced precipitation of fine Nb(C,N) has been proposed by many investigators (21-26) using several different approaches. One of the results is that the addition of Nb to austenite retards recrystallization in two distinct ways: that there is a significant delay introduced by a solute effect, and that under conditions where precipitation is more rapid than solute-retarded recrystallization, operation of the recrystallization process is prevented or retarded until precipitation is complete or nearly complete.

The conventional microalloying principle used for low carbon steel is to reduce grain size by forming microalloyed carbide or carbonitrides at ferrite grain boundaries, so reducing grain growth. The resultant fine grains show excellent Charpy toughness (crack initiation) but because of the grain boundary precipitates often give poor K_{1C} toughness values i.e., poor crack propagation resistance. In the present work the controlled rolling is done by finishing just above the austenite recrystallization temperature to produce a fine grained austenite (giving rise to excellent Charpy toughness) which is then directly quenched to produce the desired microcomposite of packet martensite and

retained austenite (giving rise to excellent K_{1C} toughness) (27).

Thus, utilizing priciples of physical metallurgy and thermomechanical treatment, this research aims at developing microcomposite structures of martensite laths and retained austenite, which have excellent mechanical properties of strength and fracture toughness using a lower chromium content of 2.0 wt% than those previously developed and increasing Charpy V-notch and K_{1C} toughnesses through thermomechanical treatment without requiring off-line heat treatment.

2. Experimental Procedures

2.1. Materials preparation

The experimental alloys used in this investigation were supplied by Pohang Iron and Steel Company in Korea. They were vacuum melted to 30 kg ingots and subsequently forged down to 75 mm thick, 75 mm wide and 330 mm long billets. They were then homogenized at 1200°C for 24 hours in a vacuum furnace before cooling. The compositions given in Table 1 were measured after homogenization. Billets were cut into 40 mm thick, 38 mm wide and 76 mm long blanks, into which thermocouples were embedded to read the exact temperature during rolling.

2.2. Thermomechanical Treatment

The blanks were austenitized at 1200°C for 75 minutes in a horizontal furnace. The austenitization temperature was determined from the experimentally obtained solubility product relationship for the microalloy element of Nb. Thermomechanical treatments were conducted on the austenitized blanks as shown in Fig.3. The first rolling of 30% reduction was done at 1100°C. The second finishing rolling was done at 950°C, 900°C and 850°C, respectively, with the same reduction of 45%. The cooling rate was also changed by quenching into water or agitated oil and by air cooling following final

rolling. Isothermal tempering treatments were done at 200°C and 250°C for 45 min.

2.3. Dilatometry

A Formastor-Digital dilatometer (Fuji Electronic Industrial Co., LTD.) was used to determine the continous cooling transformation diagrams of the experimental alloys. Specimens for dilatometry were machined into cylindrical shape with 3 mm in diameter and 10 mm in length. The specimens were austenitized at 1200°C for 3 min. and then, cooled down to room temperature with various cooling rates ranged from 40 to 0.5°C/sec as shown in Fig. 4. Thermal contraction of the specimens was plotted as a function of the temperature. The inflection points of slopes were taken as onset and finishing temperatures for phase transformation.

2.4. Mechanical testing

2.4.1. Tensile testing

The dimension of the 31.5 mm gauge round tensile specimen is shown in Fig. 5. The specimens were pulled at a cross head speed of 0.3 mm/min at room temperature. The yield strength was determined by the 0.2% offset method. Uniform elogation was taken from the elogation when the ultimate tensile strength was reached.

2.4.2. Charpy V-notch impact testing

Standard ASTM size specimens, obtained from the thermomechanically treated blanks, were used to measure the Charpy V-notch impact energy (the long axis of the test specimens was parallel to the rolling direction , and the base of the notch was perpendicular to the surface). Testing was conducted with a 224 ft-lb capacity impact machine at room temperature. Three Charpy-V-Notch specimens were testred for each treatment and the tabulated results correspond to the average of these tests.

2.4.3. Plane strain fracture toughness testing

Plane strain fracture toughness values were obtained by testing standard compact tension crack-line loaded toughness specimens shown in Fig. 5. The thickness of sample was 0.5 inch for practical interest. The Instron machine was again used for fatigue pre-cracking the specimens to a crack length of about 0.2 inch, which were subsequently tested in the same machine to obtain the fracture toughness data. The orientation of crack propagation with respect to the long dimension of the bar stock is L-T.

2.5. Metallography and Microscopy

2.5.1.Optical Metallography

Specimens for optical metallography were prepared by

grinding on wet silicon carbide paper up to 600 grit and polishing on 1 μm diamond paste. A 2% and 5% nital solution were used to reveal the martensite microstructure. For revealing prior austenite grain boundaries in fine grained specimens, etching was carried out in an etchant of 5 gm. of picric acid in 100 cc of water saturated with dodecylbenzene sulfonate.

2.5.2. Transmission electron microscopy (TEM)

Thin foils for transmission electron microscopy were obtained from the broken impact specimens. Slices of about 500 μm were cut longitudinally with an 800 μm thick abrasive wheel under flood cooling and ground down to about 125 μm. Disks of 3 mm diameter discs were cut off from these slices by mechanical punching and then carefully sanded down to about 50 μm and then electropolished in a twin jet electropolishing apparatus at -2°C in a perchloric acid - ethanol - glycerol solution at a voltage range of 12 to 15 volts and current range of 18 to 20 milliamperes. Transmission electron microscopy and diffraction were done on a Philips EM 301 Microscope operated at 100 Kv.

2.5.3. Carbon extraction replica

In order to locate the niobium carbonitride particles which were precipitated during hot rolling and to surmise the mechanism of prior austenite grain refinement, a broken Charpy bar of the niobium bearing steel was tempered intentionally for three hours at 250°C. The mounted specimen taken from the

broken Charpy bar was first etched in the same etchant, used for revelation of prior austenite grain boundaries, to expose the particles, then placed in carbon evaporating unit. The thickness of carbon was about 200 Å, judged by observing the tint of a piece of white paper alongside the specimen. The surface of the carbon deposited specimen was scored with a sharp needle in a grid pattern and then immersed in a second etching solution of 10% nital for up to 2 min. The carbon film was next floated off by immersion in distilled water, collected on a copper grid, and examined in a Philips 400 TEM with energy dispersive X-ray analysis system. Extracted particles were then idenfied by electron diffraction and chemically analyzed by X-ray fluorescent analysis.

2.5.4. Scanning electron microscopy and energy dispersive analysis of X-rays

Fractography was conducted on broken Charpy specimens, using a scanning electron microscope operated at 25 kv. Microanalysis was done using the Philips EM400 electron microscope interfaced with a Kevex 7000 system. Microdiffraction was performed using the Philips EM400 electron microscope in the TEM mode. Microanalysis was done by energy dispersive X-ray analysis (EDXS) generated by the interaction of the electron probe with the specimen, giving rise to determination of microalloyed precipitates.

3. Results

3.1. Continuous cooling transformation

In most industrial heat-treating operations a knowledge of the microstructure and hardness of the steel after continuous cooling from some temperature in the austenite region is highly desirable. Such information cannot be obtained directly from an isothermal transformation diagram, so it has been necessary to develop continous cooling transformation diagrams. These are determined by dilatometry, hardness measurements, and examination of microstructures. In dilatometry, temperature and specimen length are recorded automatically.

The martensitic transformation temperatures M_s and M_f obtained by dilatometry are shown in the Fig. 6. The higher M_s and M_f temperatures in these experimental alloy steels are attributed to the somewhat lower carbon content and lower alloy content compared with the previous work dealing with higher carbon and alloy content (8,28). In general, both the M_s and M_f temperatures tend to decrease with increasing alloy additions (29). The austenite stabilizing elements like manganese reduce the undercooling by lowering the Ac_3 temperature, and hence the driving force for transformation of austenite, at any lower temperture. This effect increases hardenability. On the same basis, ferrite stabilizing elements like chromium, because they increase undercooling, would be expected to decrease

hardenability, but most ferrite stabilizing elements tend to segregate between austenite transformation products than do the austenite stabilizers. The rate of austenite transformation is thereby delayed by diffusion of solutes. It has the effect of decreasing the M_S and M_f temperatures. As can be seen in the two continous cooling transformation digrams, niobium, even though its addition is slight, has a strong effect of shifting the ferrite and bainite "noses" to increased time, i.e., increasing martensitic hardenability.

Although the mechanism of this effect will be discussed in the subsequent chapter, precipitation or clustering of niobium can be thought to exert the drag force on advancing γ - α interface boundary. This result is extremely important in the actual production stage in steel plant. Niobium alleviates the stringent quenching condition required for processing of these experimental alloy steels to obtain the microcomposite structure.

Figure 7(a). shows an optical microstructure of packet martensite, which was quenched at the rate of 20°C/sec, and Fig. 7(b). represents a composite microstructure of martensite and bainite, whose quenching rate was 5°C/sec, and Fig. 7(c) (1.5°C/sec) and 7(d) (0.5°C/sec) show microstructure containing proeutectoid ferrite and some pearlite mixed with martensite and bainite.

3.2. Microstructural characterization

3.2.1. Optical Metallography

Optical metallography was carried out with the intention of recording any variations in the gross features of microstructure and prior austenite grain size etc. in relation to the various thermomechanical treatments for the basic quaternary alloy steel and the niobium bearing alloy steel. Figure 8(a) shows prior austenite grains of the Nb bearing alloy which was austenitized at 1200°C for 75 min and Fig. 8(b) shows prior austenite grains of the Nb bearing alloy which had 30% reduction at 1100°C after austenitizing at 1200°C. Average sizes are 250 μm and 100 μm. No observable differences can be perceived in the optical microstructures which represent the typical packets of martensite laths which were identified with transmission electron microscopy of thin foils. The lath morphology of substructure of steel martensite is important in relation to the toughness of martensitic steels. The crystallography of martensite laths and the way of obtaining this morphology depend on the alloy chemistry and thermomechanical treatments and will be discussed in the later chapter. The prior austenite grain size of the blanks after reheating treatment is directly related to the final austenite grain size of steel before phase transformation. It is affected, during reheating, by holding time and reheating temperature. And it is also influenced by the presence of microalloy element precipitates. Any microalloy element precipitates, which are undissolved in the matrix during

reheating at the austenitizing temperature, restrict grain boundary motion and influence the initial grain size. However, these undissolved microalloy element precipitates do not play the role of grain refinement during rolling process. They also detract from hardenability, and can be sites for fracture initiation. Thus undissolved carbides are not wanted. Niobium in this experiment is added for achieving prior austenite grain refinement during rolling operation and should be dissolved in the matrix after reheating. Therefore, the determination of the reheating temperature and holding time is influential in prior austenite grain size. The reheating temperature was determined by the experimentally obtained solubility product relationship of the niobium carbonitride and was confirmed by analyzing the undissolved particles using energy dispersive microanalysis. Electron photomicrographs will be shown later. Niobium did not produce the effect of reducing the recrystallization austenite grain size after rough rolling. This implies that undercooling at the deformation temperature is not high enough to induce grain refinement effect of niobium carbonitride particles.

Figure 9 show the optical microstructures of the basic quaternary alloy and the niobium bearing steels, finish-rolled at 900°C and oil quenched after rolling. These are the typical fine packets of lath martensite which are identified with transmission electron microscopy and shown later. These structures did not reveal any proeutectoid or isothermal decomposition products. It can be seen that the packet size of

niobium bearing steel is smaller than that of the basic quaternary alloy steel. This result can be thought to arise from the prior austenite grain refinement of the niobium bearing steel. Figure 10 shows the prior austenite grains, seen by scanning electron microscopy, of the thermomechanically treated steels. The average prior grain size of the base quaternary alloy which has accepted 45% reduction at 900°C is 35 μm, and that of the niobium bearing alloy is 19 μm. This refinement of prior austenite grain comes from strain induced precipitation of niobium carbides which interact with recrystallized austenite grain boundaries and inhibit the growth of the austenite grains. The mechanism of this interaction will be discussed in detail in the subsequent chapter and the identification of niobium carbonitride precipitate will be shown later. Figure 11 shows packet martensite of the basic quatenary alloy steel which was finish-rolled at 850°C. Prior austenite grains are seen to be elongated because the finish rolling was done below recrystallization temperature. Figure 12 shows the microstructure of air-cooled basic quaternary alloy steel, which consists mainly of proeutectoid ferrite and upper bainite.

3.2.2. Transmission electron microscopy

Structural characterization by transmission electron microscopy was done on as-quenched as well as quenched and 250°C tempered conditions of the basic quaternary alloy and the niobium bearing steels. In this section only the martensite

substructuire and the carbide precipitation are covered. As has been stressed in the introduction, the morphology and the substructure of steel martensite is critical to the toughness of the steel. Therefore, carefully selected diffraction pattern and dark field analyses have been carried out to detect thin films of retained austenite and carbide particles.

Figures 13 and 14 show the transmission electron micrographs of the basic quaternary alloy and the niobium bearing steels which have been finish rolled at 900°C and quenched in the water. The parallel lath morphology of martensite in all the alloys is evident as shown in bright field images. It can be seen that the martensite laths are heavily dislocated. Twinning was never observed in these experimental alloys as shown in the figures. The substantial amount of autotempered carbides can be seen in the electron micrograph consistent with the high M_S temperatures. These carbide particles are about 300 Å wide and about 0.5 μm long. Dark field image shows thin films of retained austenite. The picture is taken from [200] reflection of retained austenite. The retained austenite is confirmed by the selected area diffraction pattern. The diffraction pattern shows that the relationship between martensite laths and retained austenite is the Kurdjumov-Sachs relation. This means that the slip direction viz. [111] of martensite is parallel to that of austenite viz. [110]. This is important in toughness because it ensures continuity of plastic flow across both phases. Figure 15 shows transmission electron

micrographs of the niobium bearing steel which has been finish rolled at 950°C and quenched in the boiling water (the temperature was kept at 97°C). It can be seen that carbide particles have grown longer due to slower quenching rate and holding at boiling water temperature. The dark field image shows grown cementite.

Figures 16 and 17 show transmission electron micrographs of the basic quaternary alloy and the niobium bearing steels which have been temper treated at 250°C after accepting the same thermomechanical treatment as above. Tempering at 250°C resulted in well established $<110>_{\alpha}$ widmanstätten cementite platelets in both alloys. These cementite platelets are about 200 Å wide and 0.5 μm long. The influence of Nb can not be discerned from a comparison of electron micrographs of the basic quaternary alloy and the niobium bearing steels. Retained austenite can be detected in these tempered structures as shown in Figures 18 and 19. This means that the retained austenite in this alloy is thermally stable at 250°C. The diffraction pattern shows that the relationship between martensite laths and retained austenite is the Nishiyama-Wasserman relation. This means that the [001] direction of martensite is parallel to the [011] direction of austenite. The stability of retained austenite will be discussed in the subsequent charpter in relation to tempered martensite embrittlement.

3.3. Mechanical properties

3.3.1. Tensile properties

The mechanical properties of the basic quaternary alloy (non Nb alloy) and the niobium bearing steels are summarized in Tables 2 and 3. Tensile strength variations depended on finish rolling temperatures and cooling rates as are plotted in Fig. 20. The tensile strengths of the niobium bearing steel tend to show lower values than the basic quaterrnary alloy steel. The high strength level for the basic quaternary alloy is presumably due to somewhat higher carbon content than the niobium bearing steel as shown in Table 1. However the differences are not significant in terms of general property requirements. A substantial increase in tensile strength of the base quaternary alloy steel which was finish-rolled at 850°C can be noticed. This arises from the fact that finish rolling has been done below the recrystallization temperature and thus dislocation density has been increased considerably.

Figure 21 shows the effect of niobium on the ductility of the basic quaternary alloy. Niobium also contributes to improve the ductility.

3.3.2. Fracture properties

Figure 22 is a plot of Charpy V-notch impact energy as a function of finish rolling temperature to illustrate a comparison of Charpy V-notch impact energy of the basic quaternary alloy and the niobium bearing steels in the as-quenched condition. It

can be seen that Charpy V-notch impact toughness has been greatly improved due to the addition of the niobium to the basic quaternary alloy. The difference in Charpy V-notch impact energy is about 15 joules. The mechanism of this improvement of Charpy V-notch impact toughness will be discussed in the subsequent chapter in detail. Figure 23 is a plot of Charpy V-notch impact energy as a function of tensile strength of both steels. The niobium bearing steels give superior Charpy V-notch impact toughness compared with the basic quaternary alloy at a given strength level. Finish rolling at 850°C shows a substantial decrease in Charpy V-notch impact energy because finish rolling has been done below the recrystallization temperature. Figure 24 is a plot of Charpy V-notch impact energy of the tempered steels with and without niobium. Tempering at 200°C also contributes to the increment of Charpy V-notch impact energy. However, it is not such a great improvement as has been attained by the addition of niobium to the basic quaternary alloy steel.

Plane strain fracture toughness tests were conducted only for the as-quenched and 250°C tempered treatments because of marterial limitations as well as lack of practical interest for tempering treatments at higher than 250°C. The data from the plane strain fracture toughness testing as well as Charpy V-notch impact testing are tabulated in Tables 2 through 4. A significant improvement in the plane strain fracture toughness at a given yield strength is obtained with the niobium bearing steel, especially when compared with previous results of similar

alloys (8,28). Figure 25 shows quasi-cleavage fracture surface of the as-quenched basic quaternary alloy and Fig. 26 shows mostly ductile fracture surface of the tempered basic quaternary alloy. Figures 27 and Fig. 28 show the ductile fracture surfaces of the as-quenched and the tempered Nb bearing alloy which represent the excellent Charpy impact toughness (Fig. 22 and 24). Figure 29 shows quasi-cleavage fracture surface of air cooled Nb bearing alloy which corresponds to very low impact toughness (Table 3).

3.3.4. Microanalysis of NbC

Figure 30 shows the transmission electron micrographs of a carbon extraction replica of the niobium bearing steel which was deliberately tempered for three hours at 250°C. The bright field image shows that niobium carbonitride particles were precipitated near the grain boundary. Niobium carbonitride particle was identified by the energy dispersive X-ray analysis as shown in the figure. Although Nb is easily resolved, neither carbon nor nitrogen can be detected in such small particles. However, from previous research it can be concluded that these particles are carbonitrides. It was also confirmed by microdiffraction pattern, for example Fig. 30(c) shows the [001] fcc structure. Dark field image was taken from the [110] reflection of the particle (30). The average size of the carbonitride particles is about 100 Å.

4. Discussion

4.1. Continuous Cooling Transformation Diagram

The phase transformation kinetics of steels are mainly dependent on the alloy chemistry, the cooling rate from the austenite phase, and the prior austenite grain size prior to transformation. The effect of grain size on hardenability can be explained on the basis of the heterogeneous manner in which pearlite nucleates at austenite grain boundaries. The formation of pearlite in the fine-grain steel is, therefore, more rapid than it is in the coarse-grain steel, and accordingly, the fine-grain steel has a lower hardenability.

The hardenability of a steel is strongly influenced by its carbon content. Increasing carbon content is associated with an increase in hardenability because the formation of pearlite and proeutectoid constituents becomes more diffrcult the higher the carbon content of the steel. Other chemical elements in steels increases the hardenability to the extent that they are soluble in iron. Therfore, it can be expected that a reduction in carbon and alloy contents of the basic quaternary alloy in this investigation, results in a decrease in martensitic hardenability. It can be seen that a small addition of niobium to the basic quaternary alloy has greatly increased the martensitic hardenability of steel as shown in Fig. 6, even for the slightly lower carbon composition (Table 1).

The usefulness of niobium as a microalloy element in

thermomechanical processing has been widely studied. However, its effect on phase transformation behavior has not. Kirkaldy et al. (31) and Aaronson et al. (32) launched the first theoretical studies on the growth behavion of proeutectoid ferrite (α) in alloy steels. They introduced the concept of "no-partition Ae_3 temperature" to explain the effect of chemical element on the growth of proeutectoid ferrite. It was claimed that any chemical element which increase Ae_3 temperature than the one taken from Fe-C phase diagram can make carbon partitioning in austenite. Carbon partitioning results in a increase of growth rate of proeutectoid ferrite. Al and Co assist in carbon partitioning and promote growth of proeutectoid ferrite. Ni and Mn, on the contrary, decrease no-partition Ae_3 temperature and inhibit growth of proeutectoid ferrite. However, Mo showed totally inconsistent behavior with this theory. Mo is a ferrite stabilizer and is supposed to increase no-partition Ae_3 temperature. Nontheless, Mo considerably inhibits growth rate of proeutectoid ferrite.

Kinsman and Aaronson (33) explained this phenomenon of Mo based on a solute drag model, which is widely used in analyzing the dragging effect of solute element on grain boundary migration. Gray and Yeo (34) observed that Nb(C,N) particles precipitated at α/γ interface retards the migration of such α/γ interface. Eldis and Hagel (35) investigated the hardenability effects of Nb through varying its concentration in a basic Si-Mn

steel. It was observed that initial small additions of Nb remarkably increased hardenability, with further additions resulting in a hardenability decrease. Kobayashi et al. (36) examined the influence of Nb on the formation kinetics and growth rate of proeutectoid ferrite. They observed that the nucleation and growth rate of proeutectoid ferrite in the experimental alloy containing Nb are greatly retarded. It can be thought that the size of Nb is considerably greater than Fe and Nb is trapped in austenite grain boundary or other defects as dislocations. This can result in a decrease in stored strain energy and thus a increase in activation energy for the formation of proeutectoid ferrite. Therefore, Nb can be concluded to inhibit nucleation of proeutectoid ferrite rather than to retard growth. Nb(C,N) particles precipitated in austenite grain exert a pinning force on the α/γ interface. However, the inhibition of proeutectoid ferrite growth by pinning can not surmount the promotion effect of proeutectoid ferrite growth arising from a decrease in soluble Nb content.

4.2. Thermomechanical processing of microalloyed steel

Grain refinement has been best exploited to achieve better toughness properties of high strength, low alloy steels as has been explained in the previous chapter. Therefore, a great deal of research efforts have been made to refining austenite grain size by studying recrystallization behavior of austenite and the

interaction between microalloy element precipitation and recrystallization during hot deformation. A thorough understanding of those subjects is instrumental in alloy design and to establish the rolling schedule. Grain refinement can be accomplished by controlling the austenite grain size prior to rolling, reducing the austenite grain size during rolling and increasing the nucleation rate of transformed products during phase transformation.

The effect of the reheated grain size on the recrystallization of austenite during rolling could have a marked effect on the size and uniformity of grains in the final product. Tanaka and Kozasu (37), illustrated how rapidly the critical reduction necessary for recrystallization increased with increase in initial grain size. The importance is that coarse-grained slabs need an excessive amount of reduction at high temperatures to effect the complete recrystallization necessary to produce a uniform grain structure in the product.

Cuddy (38) found that limiting the reheated grain size by lowering the reheat temperature or by adding Ti to the steel is essential to assure complete recrystallization and refinement of initial grain structure without an excessive amount of reduction at high temperatures. But TiC is difficult to put into solution (39). Sekine and Kozasu (40-42) investigated the effect of initial grain size before rolling on the recrystallization behavior. By reducing the starting grain size, critical reduction for the onset of dynamic and static recrystallization decreased. Machida et al.

(43) investigated the effect of strain rate on the size of austenite grain recrystallized immediately after rolling in the temperature range of 1050°C to 1200°C. It was found that recrystallized austenite grains are refined by an increase in strain rate with higher rolling speed and thinner slab thickness. The experimental results showed that recrystallized austenite grain size is inversely proportional to the square root of strain rate.

Machida et al. (43) studied the influence of alloying elements on austenite recrystallization in microalloyed steels. Previous works indicated that the addition of Nb inhibits particularly the progress of recrystallization. Their experimental results suggested that the addition of alloying elements such as niobium, vanadium, and molybdenum hardly affects the austenite recrystallization at temperature higher than 1050°C, where austenite grains are recrystallized immediately after hot rolling.

Austenite grain size prior to rolling is determined by reheating conditions which also control the amount of microalloy element taken into solution. It is important for obtaining smaller final austenite grains after rolling. The smaller starting austenite grain size also makes it easier to attain recrystallization with lower reduction and results in the smaller final austenite grains. The microalloy element dissolved in the austenite is able to play the role of reducing the prior austenite grain size during rolling. Solubility of the microalloy elements depends on the thermodynamic stability of the carbonitrides and

on the kinetics of dissolution of particles present.

Nordberg and Aronson (44) calculated the solubility of niobium carbide in austenite from thermodynamic data. His data agree within the estimated error with the value determined experimentally. Because of the limited accuracy of the thermodynamic data the experimental value is the more accurate one. They discussed the composition of the niobium carbide in equilibrium with austenite and considered this particularly in interpreting previous experimental results. It was concluded that, at a C/N ratio below about five, a carbonitride rather than a carbide was precipitated. This might explain the low values of the solubility of niobium in very low carbon steel. Apparently the C/N ratio must be taken into consideration when discussing the precipitation of niobium carbide in steels with low carbon contents.

Thermodynamic stability of microalloy element is normally represented by the solubility product as a function of temperature:

$$\log (M) (X)^{y} = A - B/T \qquad (3)$$

where M is the content (wt%) of microalloy element, e.g. Nb, V, Ti or Al; X is the content (wt%) of C and N; y may be 1 or less; A and B are constants and T is absolute temperature. Parameters A and B differ widely for different carbides and nitrides. In steels with C/N > 10 experimentally determined solubility relationship by Irvine et al. (45) is widely recommended. The data were determined using chemical analysis techniques for soluble and

insoluble niobium, carbon and nitrogen and is represented by the equation:

$$\log_{10} [Nb] [C+ 12N/14] = -6770/T + 2.26 \quad (4)$$

where [C + 12N/14] represents carbon equivalent, i.e. the nitrogen content is considered in terms of an equivalent carbon content. When the niobium bearing steel used in the current investigation is heated upto 1200°C, the above equation predicts that 0.019 wt% Nb can be dissolved in austenite in case of 0.24 wt% carbon content. The niobium content added to the steel in this work was determined on the basis of the above experimental relationship. Particle size also affects the solution temperature given by this equation. Large particle is expected to have a high solution temperature whereas small particles can be dissolved at lower temperature than given by this equation. High heating rates and long holding times diminish the particle size effect.

During rolling austenite grain can be refined by repeated recrystallization between passes. This occurs relatively quickly at high temperatures and may be slow at low temperatures. As temperature decreases, an increase in incubation time for recrystallization and a decrease in the subsequent recrystallization rate occur, and because of the reduction of solubility limit of the microalloy element, the latter tends to precipitate in the austenite. The greater is the undercooling, the higher is the driving force . However, the diffusion coefficient becomes smaller as the termperature of austenite decreases. The start and the finish of precipitation of microalloy element can be

represented by the C curve (i.e. nucleation and growth rate curve) in temperature-time coordinates as has been explained in the previous chapter. Plastic deformation introduces new and potent nucleation sites which have the effect of shifting the C curve to shorter times. If precipitation starts before recrystallization, it retards recrystallization of austenite or inhibits the growth of recrystallized grains depending on the amount of the precipitated particles. The precipitation/recrystallization interactions are sensitive to the degree of supersaturation of the temperature interval between solution temperature of niobium carbonitride and post-rolling holding temperature. For example, 0.03 wt% Nb in solution is sufficient for strain-induced precipitation to retard recrystallization of hot rolled austenite at 900°C, whereas 0.02 wt% Nb is not sufficient to retard recrystallization. But it can inhibit the growth of recrystallized austenite grains as in this investigation. It was suggested that a critical degree of supersaturation may have to be exceeded, given the hot rolling conditions adoped here.

Understanding the recrystallization phenomenon is important to attain the fine austenite grain as has been stressed in the previous chapter. Recrystallization is defined as the reorientation of the crystals in a solid body by the passage of a high angle boundary. The kinetics of the process resembles that of a phase transformation, in that it often can be described in terms of nucleation frequency and a rate of growth. When we use the term "nucleation" with respect to recrystallization we do

not mean that small, strain free grains are formed by the classical process of atom-by-atom accretion until a critical size is obtained. Rather, new grains are formed by the growth of specific lattice domains already present in the deformed metals. When a deformed material is in high temperature, dislocation cells become subgrains by a process of recovery. If the cells are not present initially, they can be created by dislocation arrangement during recovery. The growth of subgrains occurs at several favored sites, these being preexisting grain boundaries, inclusions or second-phase particles, in the interior of grains and intersections of mechanical twins. The common feature of these sites is that they are all local regions of severe lattice bending. One of the characteristics of recrystallization of hot worked structures is the absence of nucleation within grains, except when inclusions are present.

Recrystallization during hot rolling can be divided into static recrystallization and dynamic recrystallization as have been introduced in the introduction. The condition for the occurrence of dynamic recrystallization is that critical strain has to be reached. And that critical strain varies with deformation temperature and strain rate. Low deformation temperature and high strain rate require too high a critical strain to induce the dynamic recrystallization. In actual plate rolling operation, the strain rate is in the range of 1 - 10^2/sec. Therefore, a rolling reduction of about 20% per pass in actual operation can not generate the dynamic recrystallization.

On holding deformed structures at high temperature, softening takes place as a function of time. Static recrystallization kinetics are affected by the amount of deformation, deformation temperature, and strain rate which are controlling variables in rolling process for austenite grain refinement. As the amount of deformation increases in the recrystallization region, austenite grain is refined. However, deformation temperature is almost independent of recrystallized grain size in the static recrystallization region (46).

A le Bon et al. (25) studied precipitation of niobium carbonitride during and after deformation in a 0.04 wt% Nb containing low carbon steel, with particular emphasis on the influence of precipitation on the static and dynamic recrystallization of austenite. Torsion testing was used over a wide range temperature, strains, and strain rates. They found out that Nb carbonitride existing before any high temperature deformation did not prevent austenite recrystallization and very fine Nb carbonitride particles formed in strained austenite can prevent static recrystallization.

Weiss and Jonas (23) measured precipitation kinetics of niobium carbonitride in 0.035 wt% Nb containing low carbon steels. A new mechanical method was employed based on the determination of the strain to the peak stress in high temperature compression tests. They comfirmed that, when the precipitation starting time is shorter than the recrystallization start time as estimated from solute modified kinetics, the

nucleation and growth of recrystallization is severely impeded. Furthermore, it was concluded that the occurrence of carbide precipitation can retard static recrystallization only when recrystallization is already retarded by the solute addition to prevent its initiation prior to use beginning of the precipitation process (47). Strain induced precipitation of microalloy element carbonitrides, which occurs before recrystallization, affects recrystallization kinetics by increasing the incubation time for recrystallization and by reducing recrystallization rate or by exerting a dragging force on moving grain boundary. When the time for the start of precipitaiton is longer than the recrystallization start, the recrystallization/time/temperature curve has the normal dependence of temperature. This is the case at high and low temperatures. Conversely, when the precipitation start time is shorter than the recrystallization start time as estimated from the solute modified kinetics, the nucleation and growth of recrystallization is severely impeded (47).

Precipitated particle size and number of precipitated particles during deformation are underlining variables in the interaction of precipitation with recrystallization kinetics. Luton et al. (48) observed that the average particle size of niobium carbonitride affecting recrystallization behavior was 20 nm. The number of precipitated particles is dependent on microalloy element content and deformation temperature. The particle size is determined by the amount of deformation which is related to the nucleation rate of strain induced precipitation.

With a large deformation at low temperature many fine particles precipitate at dislocations and at cell boundaries, and thus, inhibit cell formation and migration of cell boundaries by pinning their motion. If the number of fine particles is small, recrystallization can arise from migration of the cell boundaries because the restraining force is proportional to the number of particles. However, these fine particles restrict the growth of recrystallized grains when the driving force of grain growth reaches the pinning force of fine precipitated particles. In the alloy composition used in this investigation the niobium content is not too high to inhibit recrystallization. Thus we concluded niobium in this experimental steel exerts a restraining force on grain growth and thus austenite grain refinement can be obtained as has been shown in experimental results (Fig. 30). In this way Nb improves both Charpy toughness (fine grains) and K_{1C} toughness (retained austenite).

4.3. Microstructures and Mechanical Properties

One of the most important method to achieve ultrahigh strength of steel is by way of the martensitic transformation through rapid quenching from austenite to avoid isothermal decomposition products. The martensitic transformation describes any diffusionless transformation in which from start to completion of the transformation individual atomic movements are less than one interatomic spacing. Martensite is

any diffusionless transformation product, and steel martensite is simply a supersaturated solid solution of carbon in ferrite formed by shear of austenite (49).

In spite of the fact that tetrahedral interstitial site is large than the octahedral interstitial site in the ferrite unit cell, interstitial atoms of carbon and nitrogen prefer to occupy the octahedral positions in the ferrite lattice. This causes a considerable distortion and this strain can be relieved by the redistribution of carbon atoms by diffusion at room temperature. A strong binding is set up between dislocations and the carbon atoms. This restricts the motion of dislocation and is one way of increasing the strength of steel martensite (50).

The invariant plane strain condition for the martensitic transformation requires an inhomogenous shear in the product phase, which produces no net macroscopic distortion on the martensite habit plane. This requirement can be achieved by dislocation slip or twinning which determines the substructure of martensite. The substructure plays an important role in controlling the toughness of steel martensite. Several investigations in the past revealed that twinned martensite possessed much inferior toughness properties compared to dislocated lath martensite at the same strength level. Twinning reduces the available slip number of active slip systems and is detrimental to the toughness of steel and therefore, should be avoided.

The factors affecting the morphology and the substructure of

steel martensites have been the subjects of a number of researchers. The morphology of a lath with dimensions $a > b >> c$ growing on a $\{111\}_\gamma$ plane suggests a thickening mechanism involving the nucleation and glide of transformation dislocations moving on discrete ledges behind the growing front. This picture of growth is suggested, e.g. in the work of Rao (27). The criterion to be satisfied for dislocation nucleation in this case is that the stress at the interface exceeds the theoretical strength of the material at a given temperature for a particular composition.

Johari and Thomas (51) suggested that both martensitic transformation temperature and alloy composition influence the extent of twinning. Huang and Thomas (52) found that an upper limit to the addition of Mn to a 0.25 wt% C steel in order to avoid excessive amount of twinning was 3 wt%. This implies that in the presence of C, Mn is just as much a promoter of twinning as C. In the present investigation by limiting the maximum Mn addition to 1.2 wt%, twinning is avoided (Table 1). Any significant differences in lath widths with different composition and different thermomechanical treatment were not found.

Retained austenite was found in both the basic quaternary alloy and the niobium bearing steel as shown in Figs 13-19. Increasing carbon content of steels increases the volume fraction of retained austenite following quenching to room temperature. The detrimental effects of retained austenite in high carbon steels wherein it transforms to twinned martensite

under the influence of an applied load are recognized (53). A systematic experiment has been done to understand the effects of retained austenite on mechanical properties using experimental Fe/C/X ternary alloys where X is a substitutional alloying element (3,7). For a given strength level, the plane strain fracture toughness values of Fe/Cr/C steels were higher than those of Fe/Mo/C alloys. In both cases the martensite was dislocated. Transmission electron metallography showed the existence of interlath films of austenite in the former whereas austenite could not be detected in the latter. Although the contribution of retention of the retained austenite to the toughness property has been debated, experimental results of mechanical properties in this investigation clearly show that it has a beneficial effect on the fracture toughness properties (Table 4.). The carbide forming elements such as Cr, Nb, etc., due to the attractive interaction with C (in the increasing order), lower the activity coefficient for C. Therefore, they favor C partitioning and achieve austenite stabilization.

The orientation relationships between martensite lath and retained austenite shown in experimental alloys show the Kurdjumov-Sachs and the Nishiyama-Wasserman relations. The K-S and the N-W relations are related simply by a 5.26° rotation around the normal of a close packed plane in either crystal structure (54).

Although martensitic transformation is fundamental to strengthening of steel, most of the martensitic steels have to be

heat treated after the transformation in order to improve the toughness. Tempering of ferrous martensite can be divided into various stages depending on temperature ranges producing new phases. It involves ε-carbide precipitation (first stage tempering), retained austenite decomposition (second stage tempering), cementite precipitation (third stage tempering), and formation of alloy carbide (fourth stage tempering).

Retained austenite is still untransformed in the tempered steels at 250°C as shown in Figs. 18 and 19. Three mechanisms have been proposed for stabilizing the retained austenite: (1) Interstitial carbon can physically segregate from the lath martensite to the surrounding austenite and this partitioning can lower the local M_S sufficiently below room temperature whereby austenite is stabilized at room temperature (chemical stabilization). (2) Diffusion of interstitials C & N forms dislocation atmospheres to inhibit their motion. These pinned dislocations can be in the martensite/austenite interface or they can be in either phase, thus, inhibiting stress relaxation in the martensite or austenite (thermal stabilization). (3) Accomodation of plastic deformation in austenite accompanying the shear transformation and dilatation in the martensite lattice due to carbon requires additional driving force (mechanical stabilization).

On the second stage tempering , the retained austenite decomposes to give thin lath boundary films of cementite which, in case of higher concentrations of retained austenite, can be

fairly continuous along the lath boundaries. It is now known that this interlath cementite is responsible for tempered martensite embrittlement (54), frequently encountered as a toughness minimum in the range 300 - 350°C, depending on the alloy composition, by leading to easy nucleation of cracks, which then propagate across the tempered martensite laths.

Tempered martensite embrittlement is different from temper embrittlement which occurs at higher tempering temperature, approximately at 500°C and is not a microstructural effect but rather due to impurity segregation (principally Sb, Sn, Cu, etc.) to prior austenite grain boundaries leading to intergranular fracture along those boundaries. In case of tempered martensite embrittlement the fracture path is quasi-cleavage; transgranular with respect to the prior austenite grains.

Tempered martensite embrittlement is associated with the transformation of retained austenite into carbides at the lath boundaries due to its thermal instability. The main factors affecting fracture appear to be the size and distribution of the carbides (both inter- and intralath) and the effect of this microstructure on slip distribution and crack initiation. Interlath carbides, formed when the retained austenite decomposed, must restrict slip within the lath, i.e., the carbides do not allow easy crossing of slip from lath to lath, unlike the situation before retained austenite decomposes. Hence, crack initiation is also strongly influenced by the austenite decomposition. It should be noted that as far as this interlath morphology is concerned, the

situation is very similar to that of upper bainite which also consists of lath and interlath carbide stringers (55). Base upon these results, tempering above 300°C of the experimental alloy steels in this investigation has not been carried out.

As was pointed out, in ultrahigh strength steels, increasing toughness has been the major research topic in alloy designing and processing of steels. As for the evaluation of toughness, plane strain fracture toughness and Charpy V-notch impact tests are most widely used. The characteristic difference of both test methods is the notch root radius of the sample. Plane strain fracture toughness method has fatigue precracked notch the root radius of which can be considered as zero.

It has been reported that the fracture toughness K_{1C} of low alloy and high strength steels may be increased by as much as a factor of two with no loss in strength, by austenitizing at temperatures greater than 1100°C prior to quenching (56). Although a corresponding increase in Charpy impact energy might be expected, results for some ultrahigh strength steels have shown no increase or a decrease in impact energy after austenitizing at high temperatures in both the as-quenched and quenched and tempered conditions. Therefore, it is necessary to have high sharp notch and blunt notch fracture toughnesses for practical use.

Ritchie et al. (56), and Ritchie and Horn (57) have suggested that this apparent inconsistency can be explained by comparing the relative toughness of specimens austenitized at conventional

temperature (870°C) vs. higher austenitizing treatments as a function of notch root radius. They proposed models which accounts for the effect of notch acuity on toughness for stress-controlled (i.e., cleavage, quasi-cleavage and intergranular fracture modes) and strain-controlled (i.e., microvoid coalescence or ductile rupture) failures. According to the models, the toughness is proportional to the square root of the root radius independent of the type of failure. When the radius of the notch is decreased below a critical value, ρ_0 (characteristic of a given structure), the toughness is constant. The argument put forward to account for the existence of a limiting root radius is that the critical stress or strain at the crack tip must be exceeded over a greater distance than the microstructure feature which initiates failure, e.g., the plastic zone size must exceed the interparticle spacing for fibrous rupture because the decohesion of fracture of the particle (carbide) initiates failure. They explained that a increase in K_{1C}, following high temperature austenitizing, results from a significant increase in characteristic distance.

Carlson et al. (39) investigated the as-quenched sharp-notch (K_{1C}) as well as blunt-notch (Charpy) toughnesses of simple Fe/Cr/C alloys as a function of austenitizing temperature. They found that the fracture toughness, K_{1C}, does not increase with austenitizing temperature if the microstructure does not coarsen, i.e., the characteristic distance ρ_0 does not

significantly increase, and Charpy impact toughness decreases with increasing prior austenite grain sizes and increases with decreasing number of submicron particles (carbides or inclusions). Therefore, in order to obtain high fracture and Charpy impact toughnesses, it is necessary to austenitize at temperatures high enough to dissolve alloy carbides and thus, increase interparticle spacings, and to apply controlled rolling to reduce prior austenite grain size.

Experimental results on optimally rolled, water quenched and tempered samples which give plane strain fracture toughness of 155 MPa$\sqrt{m}$ in combination with a yield strength of 1200 MPa and Charpy values of about 50 joules show good promise for practical applications.

5. Conclusions

Niobium modified microcomposite Fe/C/Cr/Mn steel with reduced chromium composition was thermomechanically treated to obtain the optimized conditions which produce the best combinations of mechanical properties. The following conclusions are drawn from this study.

(1) The small addition of Nb to Fe/0.25 wt% C/2.0 wt% Cr/1.2 wt% Mn alloy increased martensitic hardenability significantly. This result makes up for the reduction of hardenability arising from lowering Cr and C contents and alleviates the stringent quenching rate required for attaining the microcomposite structure of heavily dislocated lath martensite and thin films of retained austenite.

(2) The Nb-modified Fe/C/Cr/Mn steel which had heavy deformation at 900°C showed excellent Charpy impact toughness. The benefit in Charpy impact energy is concluded to arise from grain refinement. The highest Charpy V-notch impact energy of Nb modified steel which had 45% reduction at 900°C is 48 joules. Plane strain fracture toughness of the same steel is 147 MPa$\sqrt{m}$. High plane strain fracture toughness is considered to be due to the presence of retained austenite which blunts moving cracks and causes them to branch out.

(3) The presence of NbC particles around prior austenite grain boundaryies, which were detected with transmission electron microscopy and verified with X-ray energy dispersive analysis,

authenticate the view that NbC particles act as a drag on moving austenite grain boundaries.

Acknowledgements

The author would like to extend sincere appreciation and gratitude to Professor Gareth Thomas for his continuous encouragement and expert guidance throughout the course of this investigation. He also expresses his acknowledgement to Professor Ronald Gronsky for his valuable discussion and advice. He also wishes to acknowledge Professor Frank Hauser for his review of this manuscript.

The author acknowledges Pohang Iron and Steel Company, Korea for financial support and alloy preparation for this study. Special thanks are extended to T. J. Park, the chairman of Pohang Iron and Steel Company, for his encouragement.

He would like to thank all the graduate students and research staffs in the Department of Materials Science and Mineral Engineering for the friendship and assistance.

Finally, he is grateful for his family who showed endurance during his study. He is also indebted to his mother who always prayed for his health.

References

1. F. B. Pickering, "Physical Metallurgy and The Design of Steels," Applied Science Publishing, London, 1978.

2. G. Thomas, LBL Report No. 21303, Jan., 1986.

3. G. Thomas, M. Sarigaya, G. D. W. Smith and S. J. Bernard, Advances in Physical Metallurgy of Steels, Inst. of Metals, London, 1983, p. 25.

4. R. A. Clark and G. Thomas, Met. Trans., 7A (1976), p. 831

5. G. Thomas and Y. Chen, Metal. Trans., 12A (1981), p. 933.

6. M. Sarikaya, B. G. Steinberg, and G. Thomas, Met. Trans., 13A (1982), p. 2227.

7. G. Thomas, Metal. Trans., 9A (1978), p. 439.

8. B. V. N. Rao and G. Thomas, Metal. Trans., 11A (1980), p. 441.

9. K. J. Irvine, F. B. Pickering, and J. Garstone, JISI, Vol. 196 (1960), p. 66.

10. J. McMahon and G. Thomas, Proc. Int. Conf. on Strength of Metals and Alloys, Inst. of Metals, London, 1973, Vol. 1, p.180.

11. J. D. Bolton, E. R. Petty, and G. B. Allen, Met. Trans., 2 (1971), p. 2915.

12. L. Meyer, C. Strassburger, and C. Schneider, Proc. Conf. on "HSLA Steels: Metallurgy and Applications, Nov., 1985" edited by J. M. Gray, T. Ko, Z. Shouhua, W. Baorong, X. Xishau, p. 29.

13. L. J. Cuddy, Met. Trans., 12A (1981), p. 1313.

14. M. Cohen and S. S. Hansen, as ref. 12, p. 61.

15. J. M. Gray and A. J. DeArdo, as ref. 12, p. 83.

16. C. M. Sellars, as ref. 12, p. 73.

17. C. M. Sellars and J. A. Whiteman, Met. Sci., Mar.-Apr., 1979. p. 187.

18. C. Ouchi, T. Okita, T. Sanpei and I. Kozasu, Tetsu-to-Hagane, 63 (1977), p. 53.

19. T. Tanaka, T. Hatomura, and N. Tabata, Tetsu-to-Hagane, 62 (1976), S206.

20. T. Glasman and F. B. Pickering, JISI, Jun., 1967, p. 653.

21. I. Weiss and J. J. Jonas, Met. Trans., 11A (1980), p. 403.

22. H. Watanabe, Y. E. Smith and R. D. Pehlke, "The Hot Deformation of Austenite," The Met. Soc. of AIME, New York, 1977, p. 140.

23. I. Weiss and J. J. Jonas, Met. Trans., 10A (1979), p. 831.

24. I. Weiss and J. J. Jonas, Met. Sci., Vol. 13, 1979, p. 238.

25. A. le Bon, J. Rofes-Vernis, and C. Rossard, Met. Sci., Vol. 9, 1975, p. 36.

26. A. T. Davenport, R. E. Miner, and R. A. Kot, as ref. 21, p. 186.

27. G. Thomas, J. K. Kim, and D. Manojlovic, "Development of High Strength and Toughness Microcomposite HSLA Fe/Cr/Mn/C Steel with and without Nb," presented at the Int. Conf. on HSLA steels, Pittsburgh, PA, Nov. 3-5, 1987.

28. B. V. N. Rao, Ph. D. Thesis, Univ. of Calif., Berkeley, Feb. 1978, LBL Report No. 7361.

29. W. Leslie, "The Physical Metallurgy of Steels," Hemisphere

Publishing Corporation, Washington, 1981.

30. G. Thomas and M. J. Goringe, "Transmission Electron Microscopy of Materials" John Wiley and Sons, 1979.

31. G. R. Purdy, D. H. Weichert, and J. S. Kirkaldy, Trans. AIME, 230 (1964), p. 1025.

32. H. I. Aaronson and H. Domian, Trans. AIME, 236(1966), p.781.

33. K. R. Kinsman and H. I. Aaronson, "Transformation and Hardenability in Steels," Climax Molybdemum Company, Ann Arbor, MI, 1967.

34. J. M. Gray and R. B. G. Yeo, Trans. ASM, 61(1968), p. 255.

35. G. T. Eldis and W. C. Hagel, "Hardenability Concepts with Application to Steels," Met. Soc. of AIME, 1978, p. 397.

36. H. Kobayashi, H. Kaji, and Y. Kasamatsu, Tetsu-to-Hagane, Vol. 14, 1981, p. 119.

37. T. Tanaka, Int. Met. Rev., Vol. 4, 1981, p. 185.

38. L. J. Cuddy, Metal. Trans., 15A (1984), p. 87.

39. M. F. Carlson, B. V. Rao, and G. Thomas, Met. Trans., 10A (1979), p. 1273.

40. C. Ouchi, T. Sanpei, and I. Kozasu, Tetsu-to-Hagane, Vol. 1, 1981, p. 143.

41. H. Sekine and T. Maruyama, Seitetsu Kenkyu, No. 209 (1976), p. 43.

42. H. Sekine, T. Maruyama, and Y. Kawashima, Tetsu-to-Hagane, 59 (1973), p. S636.

43. M. Machida, M. Katsumada, and H. Kaji, Proc. Int. Conf. on Steel

Rolling, Science and Technology of Flat Rolled Products, Sep. 29 through Oct. 4, 1980, Tokyo, Japan, p. 1249.

44. H. Nordberg and B. Aronson, JISI, Dec. 1968, p.1263.

45. K. J. Irvine, F. B. Pickering and T. Gladman, JISI, Feb. 1967, p. 161.

46. R. A. P. Djaic and J. J. Jonas, JISI, Apr., 1972, p. 256.

47. S. S. Hansen, J. B. Vandersande, and M. Cohen, Met. Trans., 11A (1980), p. 387.

48. M. J. Luton, R. Dorvel, and R. A. Petkovic, Met. Trans., 11A (1980), p. 411.

49. R. A. Porter and K. E. Easterling, "Phase Transformation in Metals and Alloys, Van Nostrand Reinhold Co., 1981.

50. Z. Nishiyama, "Martensitic Transformation," 1978, Academic Press.

51. O. Johari and G. Thomas, Acta Met., 13, 1965, p. 1211.

52. D. Huang and G. Thomas, Met. Trans., 2 (1971), p. 1587.

53. G. Krauss and A. R. Marder, Met. Trans., 2A (1971), p. 2343.

54. M. Sarikaya, Ph. D. Thesis, Univ. of Calif., Berkeley, Oct. 1982, LBL Report No. 15111.

55. M. Sarikaya, A. K. Jhingan, and G. Thomas, Metal. Trans., 14A (1983), p. 1121.

56. R. O. Ritchie, B. Francis, and W. L. Sewer, Met. Trans., 7A (1976), p. 831.

57. R. M. Horn and R. O. Ritchie, Met. Trans., 9A (1978), p. 1039.

Table 1. Alloy Compositions

Alloy	C	Mn	Cr	Nb	Si	P	S
Basic Quaternary Alloy	0.26	1.20	1.99	-	0.14	0.012	0.015
Niobium Bearing Alloy	0.24	1.21	1.98	0.02	0.046	0.006	0.004

Table 2. Mechanical Properties of Fe/0.25% C/1.2% Mn/2.0% Cr

First Rolling Temp(°C)/Red(%)	Second Rolling Temp(°C)/Red(%)	Tempering Temp(°C)	YS (MPa)	UTS (MPa)	Elongation Total(%)	Charpy Impact Energy(J)
1100/30	950/45	As-WQ	1208	1630	12.6	33
"	"	200				38
"	"	250	1236	1505	14.7	35
"	"	As-OQ	1139	1608	15.4	29
"	"	200				33
"	"	250	1236	1498	16.8	31
"	"	Air Cool	842	1188	15.4	4
"	900/45	As-WQ	1374	1601	13.3	29
"	"	200				35
"	"	250	1111	1456	13.3	34
"	"	As-OQ	1208	1601	16.8	26
"	"	200				31
"	"	250	1236	1519	15.4	29
"	"	Air Cool	739	1111	18.2	4
"	850/45	As-WQ	1456	1769	10.2	15
"	"	200				19
"	"	250	1312	1656	15.4	19
"	"	As-OQ	1236	1760	15.4	15
"	"	200				24
"	"	250	1284	1637	14.7	22

Table 3. Mechanical Properties of Fe/0.25% C/1.2% Mn/2.0% Cr/0.02% Nb

First Rolling Temp(°C)/Red(%)	Second Rolling Temp(°C)/Red(%)	Tempering Temp(°C)	YS (MPa)	UTS (MPa)	Elongation Total(%)	Charpy Impact Energy(J)
1100/30	950/45	As-WQ	1139	1540	16.1	46
"	"	200				52
"	"	250	1188	1485	16.1	41
"	"	As-OQ	1126	1512	16.1	42
"	"	200				46
"	"	250	1208	1485	16.8	41
"	"	Air Cool	842	1091	19.6	4
"	900/45	As-WQ	1138	1560	16.8	38
"	"	200				46
"	"	250	1188	1540	16.8	35
"	"	As-OQ	1160	1519	16.8	48
"	"	200				54
"	"	250	1160	1485	15.4	42
"	850/45	As-WQ	1160	1540	14.7	35
"	"	200				41
"	"	250	1340	1512	14.0	31

Table 4.

Plane Strain Fracture Toughness Property

Alloy	Tempering Temperature (°C)	Plane Fracure Toughness (MPa √m)
Basic Quaternary Alloy	As Quenched	132
	250	145
Niobium bearing Alloy	As Quenched	147
	250	155

Figure Captions

Fig. 1. Schematic showing desired microcomposite structure consisting of major phase martensite contributing strength and minor phase retained austenite providing improved toughness.

Fig. 2. Comparison of microalloying principles between conventional microalloying and microcomposite microalloying. Microstructures evolved from microcomposite microalloying exhibit good Charpy impact toughness and excellent plane strain fracture toughness.

Fig. 3. Schematic digram of thermomechanical treatment.

Fig. 4. Schematic diagram of heating and cooling schedule for dilatometry.

Fig. 5. Sketches of round tensile (a), fracture toughness (b), and impact toughness (c) specimens.

Fig. 6. Continuous cooling transformation diagrams of Fe/ 0.25 w% C/2.0 wt% Cr/1.2 wt% Mn with and without 0.02 wt% Nb. Niobium increases hardenability of the basic quaternary alloy by exerting a retarding role in decomposition of austenite.

Fig. 7. Optical microstructures taken from samples for dilatometry: (a) shows packet martensite (20°C/sec), (b) show composite of martensite and bainite (5°C/sec), and (c) and (d) show mixed structures of proeutectoid ferrite, pearlite, martensite, and bainite.

Fig. 8. Optical micrographs showing prior austenite grain of the Nb bearing alloy. (a) Austenitizing at 1200°C produces average grain size of 250 μm. (b), Rough rolling of 30% reduction at 1100°C reduces average grain size to 100 μm.

Fig. 9. Typical packet martensite of the basic quaternary alloy (a),

martensite laths and dark field image (b) shows Widmanstätten cementite.

Fig. 18. Transmission electron micrographs of the basic quaternary alloy which was tempered at 250°C. Bright field image (a) shows martensite laths and dark field image (b) shows retained austenite. Retained austenite still exists in microcomposite structure.

Fig. 19. Transmission electron micrographs of the Nb-bearing alloy which was tempered at 250°C. Bright field image (a) shows martensite laths and dark field image (b) shows retained austenite. Retained austenite still exists in microcomposite structure.

Fig. 20. Tensile strength vs. finishing rolling temperature of the basic quaternary and Nb bearing alloys. Higher tensile strength of the basic quaternary alloy is presumably due to lower carbon content that the Nb-bearing alloy.

Fig. 21. Total elongation vs. finishing rolling temperature of the basic quaternary and Nb-bearing alloys. Niobium contributes to the ductility.

Fig. 22. Charpy V-notch impact energy vs. finishing rolling temperature of both alloys in as-quenched condition. The Nb-bearing alloy has remarkable increase in Charpy impact toughness due to prior austenite grain refinement.

Fig. 23. Charpy V-notch impact energy vs. tensile strength of both alloys. Charpy impact toughness of the Nb-bearing alloy is much higher thatn the basic quaternary alloy at the same strength level.

Fig. 24. Charpy V-notch impact energy vs. finishing rolling temperature of both alloys in tempered condition (250°C). Tempering contributes increment of Charpy impact toughness but it is slight.

Fig. 25. Scanning electron micrographs of the basic quaternary alloy which was finish rolled at 900°C. (a) is from water quenched sample and (b) is from oil quenched sample. Both show mostly quasi-cleavage fracture surface.

Fig. 26. Scanning electron micrographs of the basic quatenary alloy which was tempered at 250°C. (a) is from water-quenched sample and (b) is from oil-quenched sample. Both show mixed fracture mode of quasi-cleavage and ductile rupture.

Fig. 27. Scanning electron micrographs of the Nb bearing alloy which was finish rolled at 900°C. (a) is from water-quenched sample and (b) is from oil-quenched sample. Both show mostly ductile rupture.

Fig. 28. Scanning electron micrographs of the Nb bearing alloy which was tempered at 250°C. (a) is from water-quenched sample and (b) is from oil-quenched sample. Both show ductile rupture.

Fig. 29. Scanning electron micrographs of air cooled Nb-bearing alloy showing typical quasi-cleavage fracture.

Fig. 30. (a) is bright field image of NbC around grain boundary of the Nb bearing alloy which was deliberately tempered for 3 hours at 250°C. (b) is dark field image of NbC particles. (c) is microdiffraction pattern of [001] fcc structure of NbC. (d) is energy dispersive analysis of X-rays obtained from the same particles in the dark field image (c).

Composite microstructure

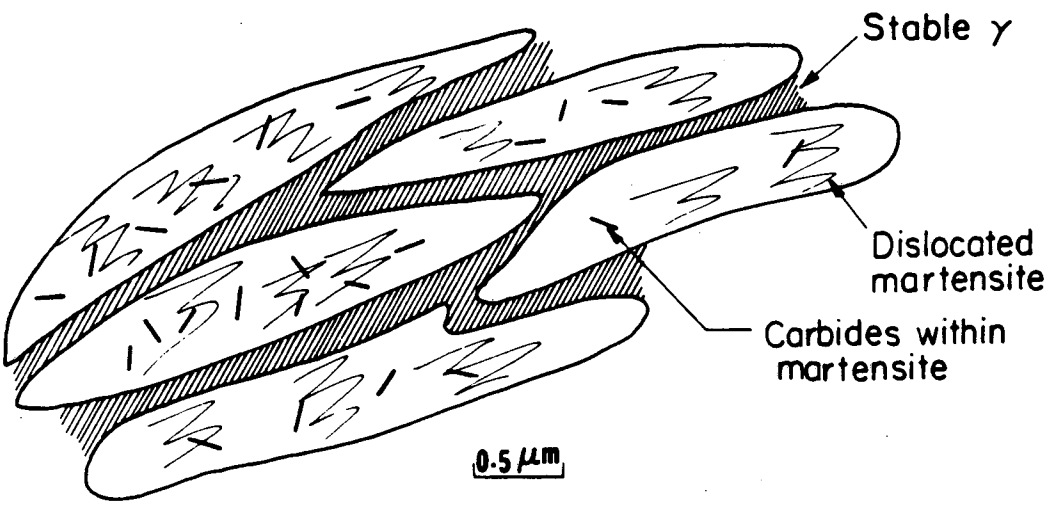

Fig. 1

Difference in microalloying principles

	Schematic digrams of controlled rolling	Evolutions of microstructure	Results
Conventional microalloying	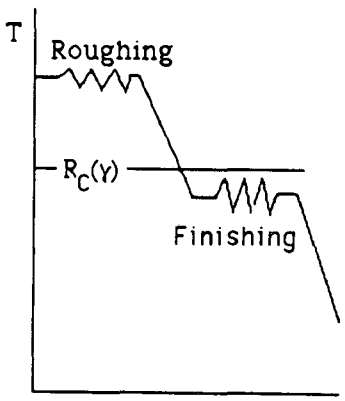	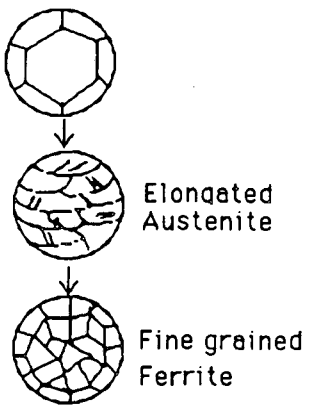	Low C Good C_v Poor K_{Ic}
Microcomposite microalloying	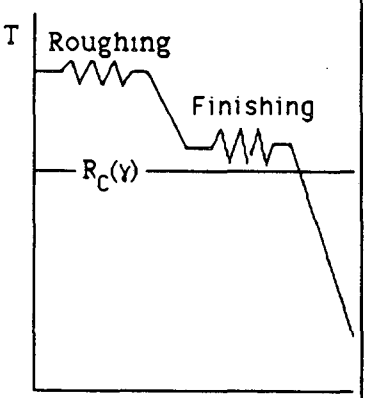	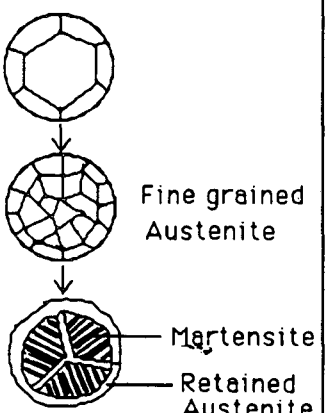	Ultrahigh strength Good C_v Excellent K_{Ic}

XBL 8811-3774 A

Fig. 2

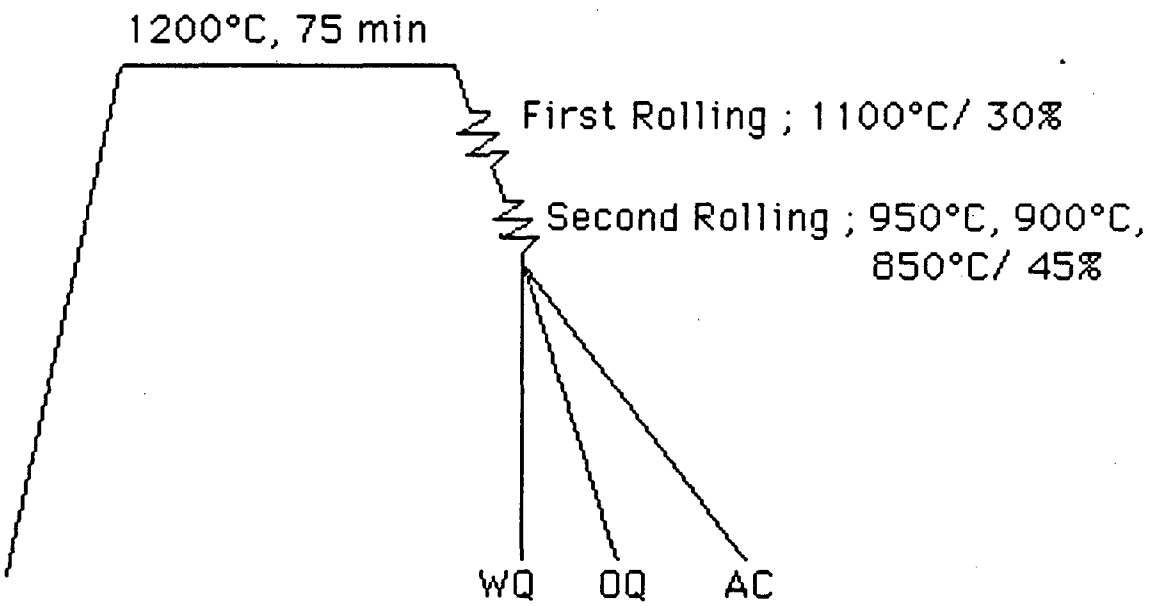

XBL 8811-3776 A

Fig. 3

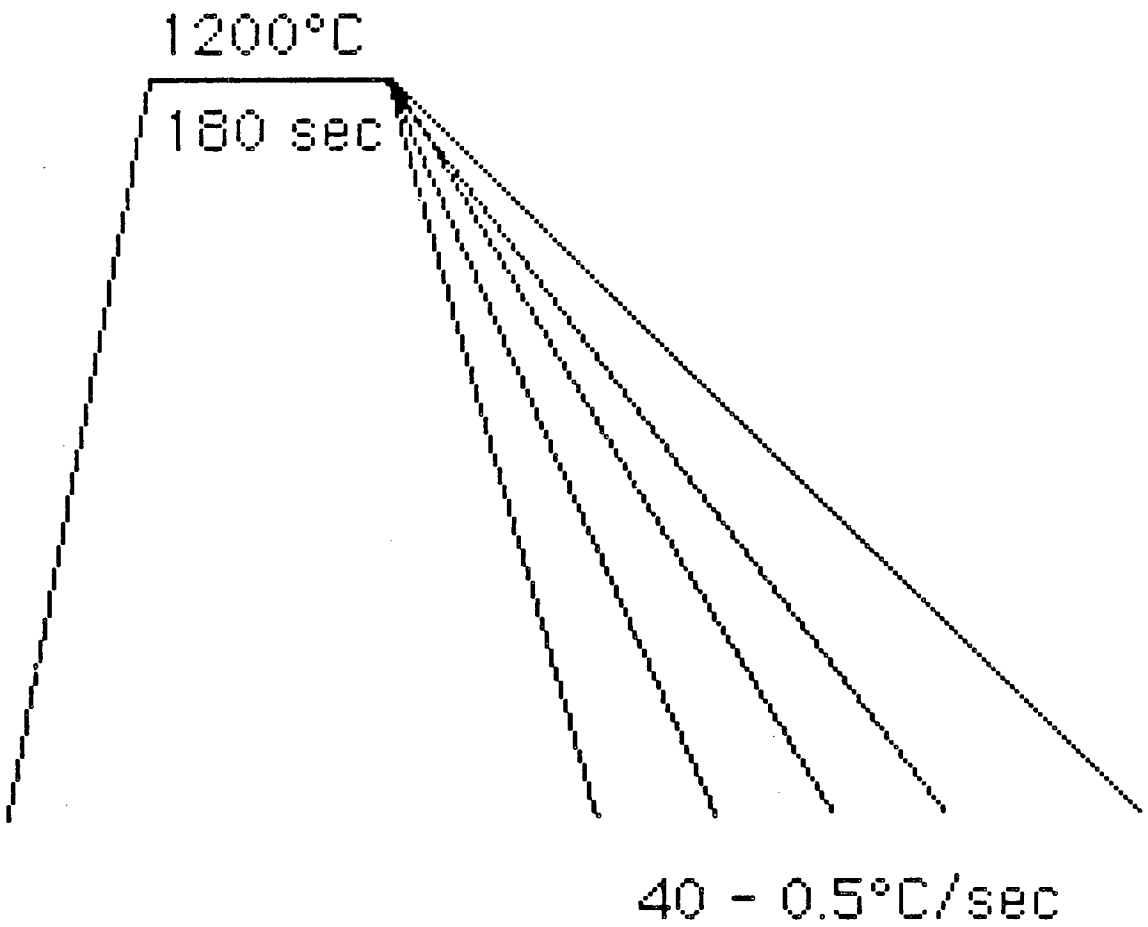

XBL 8811-3783 A

Fig. 4

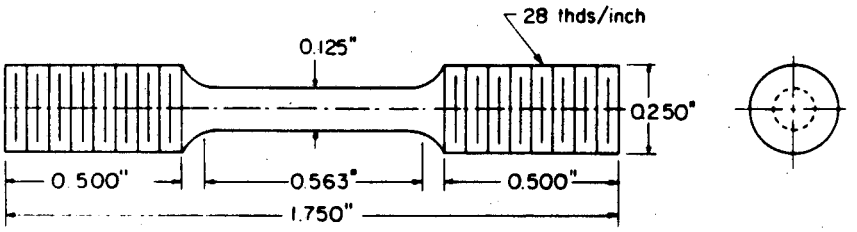

A. TENSILE SPECIMEN

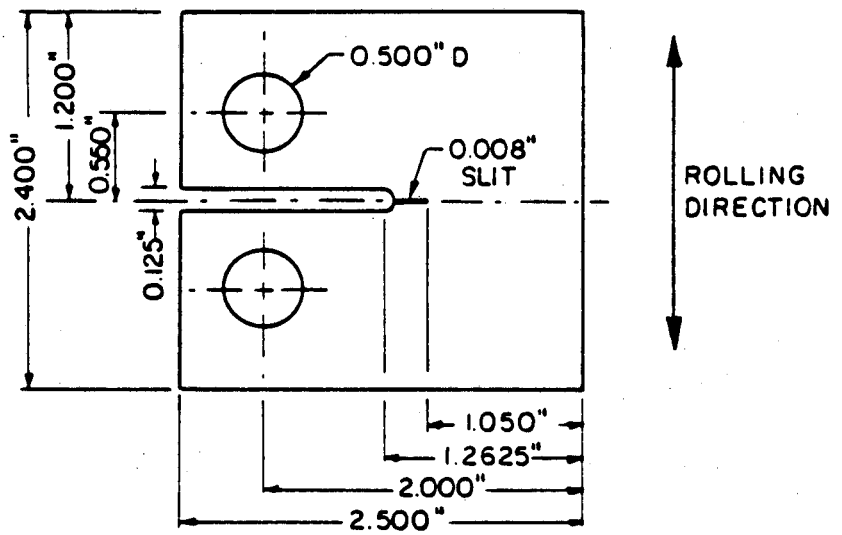

B. FRACTURE TOUGHNESS SPECIMEN

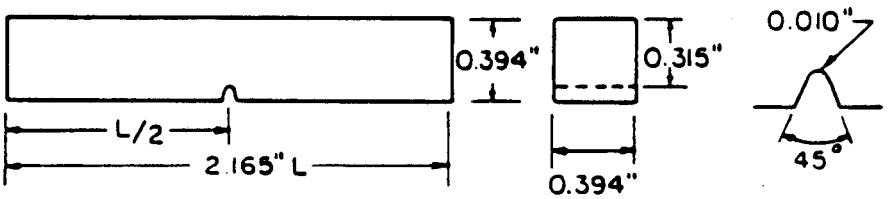

C. CHARPY V-NOTCH IMPACT SPECIMEN

XBL 8811-3777 A

Fig. 5

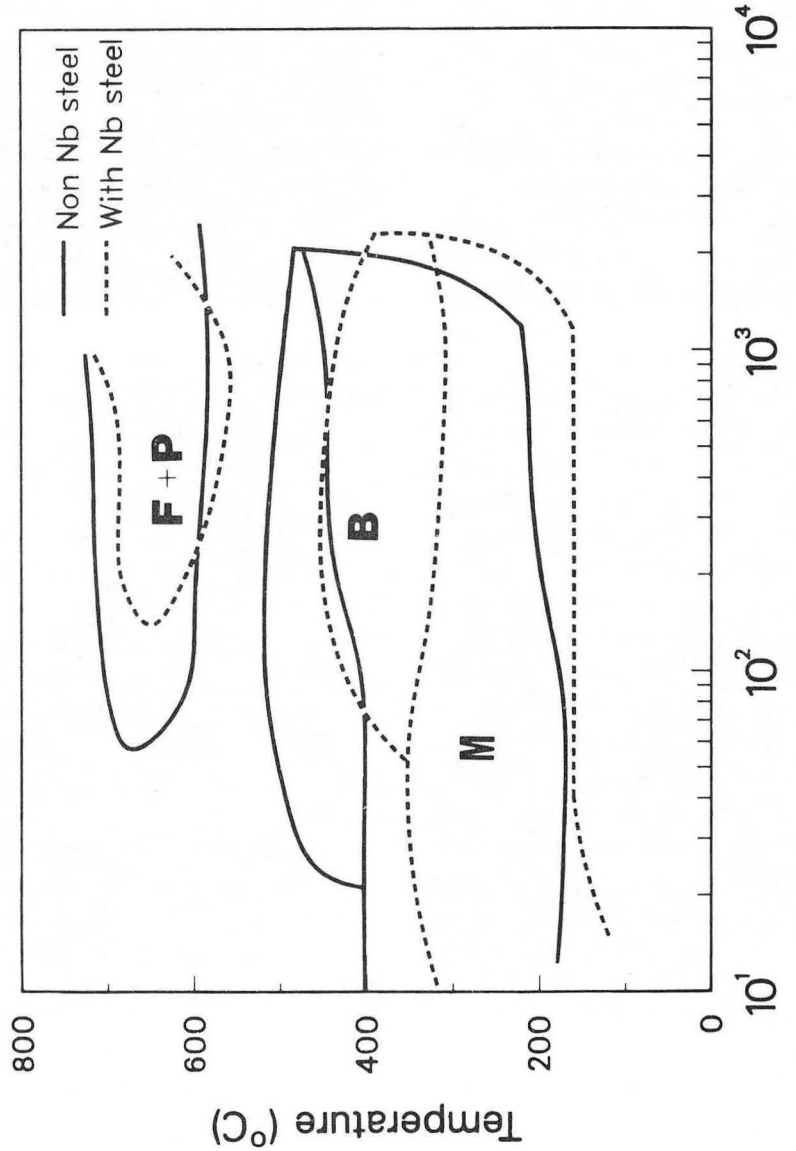

XCG 8710-11438 A

Fig. 6

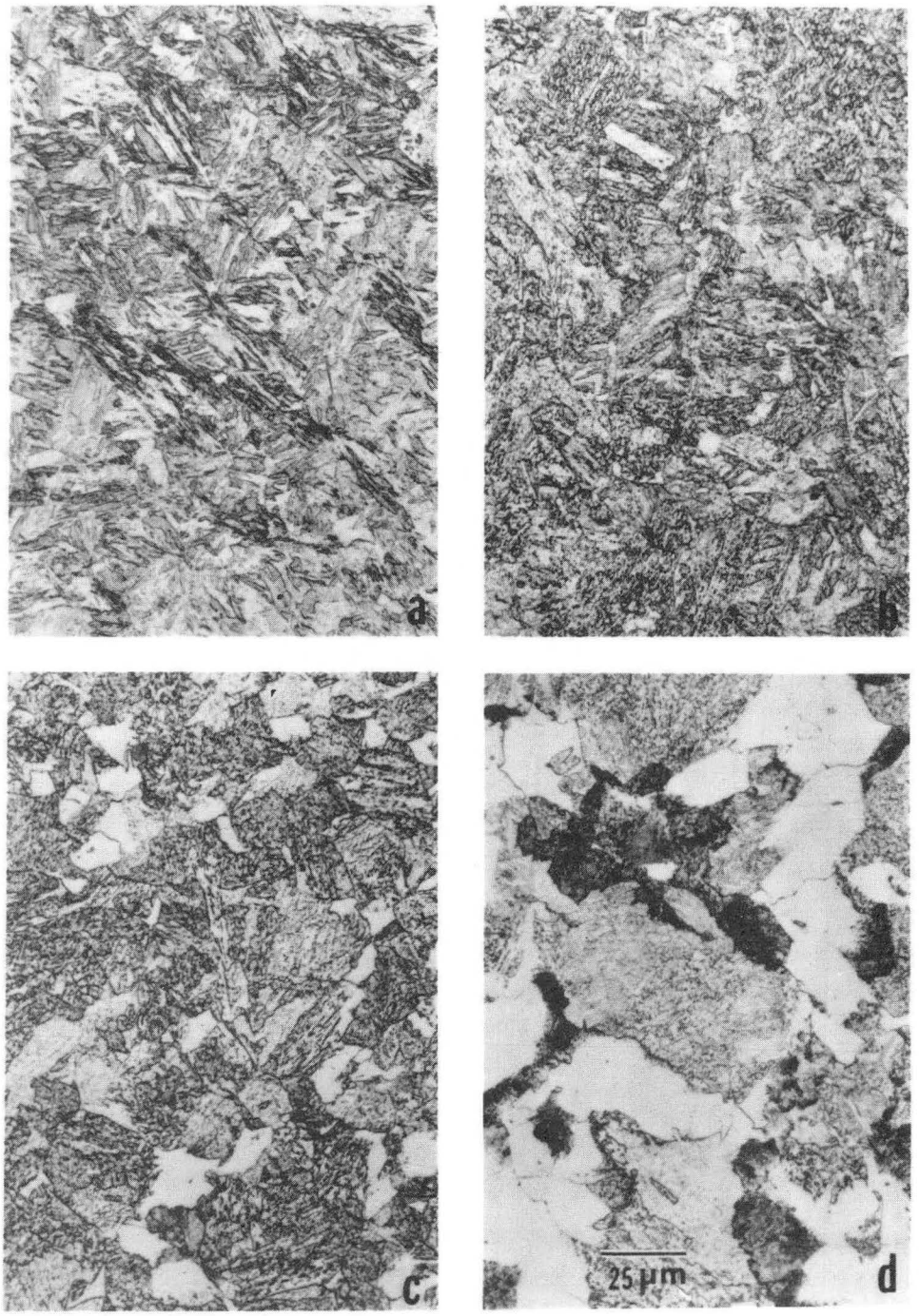

XBB 881-471 B

Fig. 7

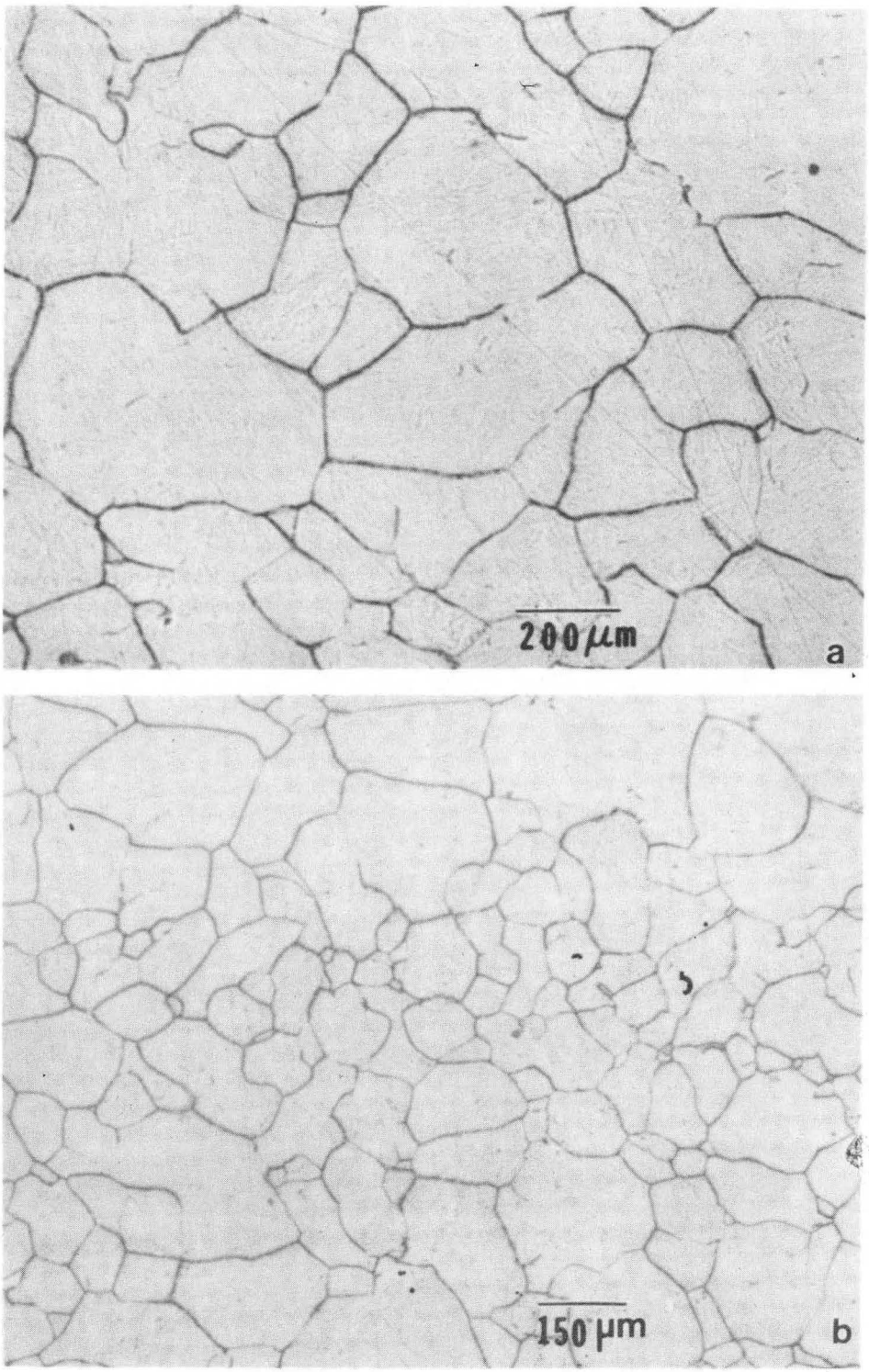

XBB 880-10530 A

Fig. 8

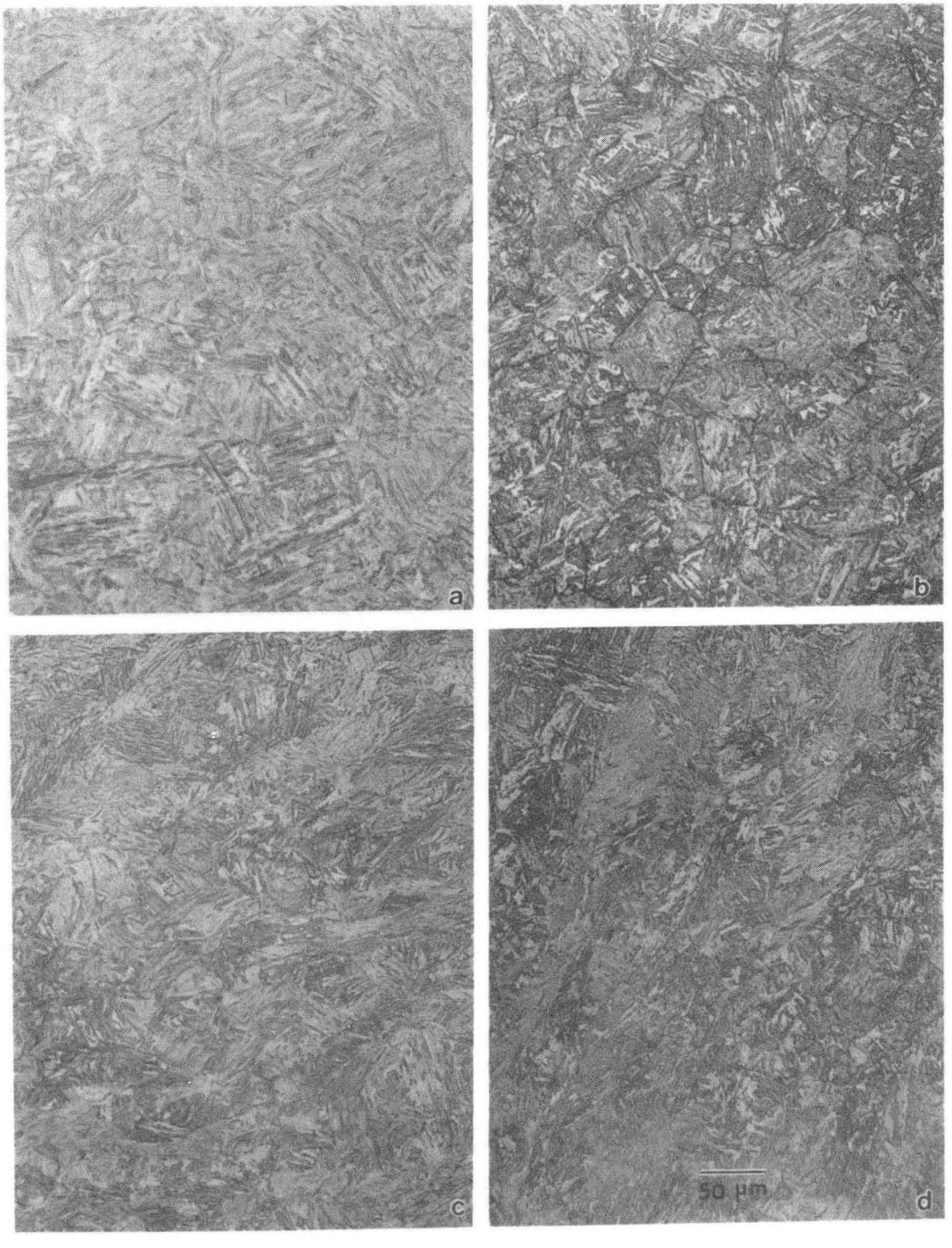

XBB 880-10529 A

Fig. 9

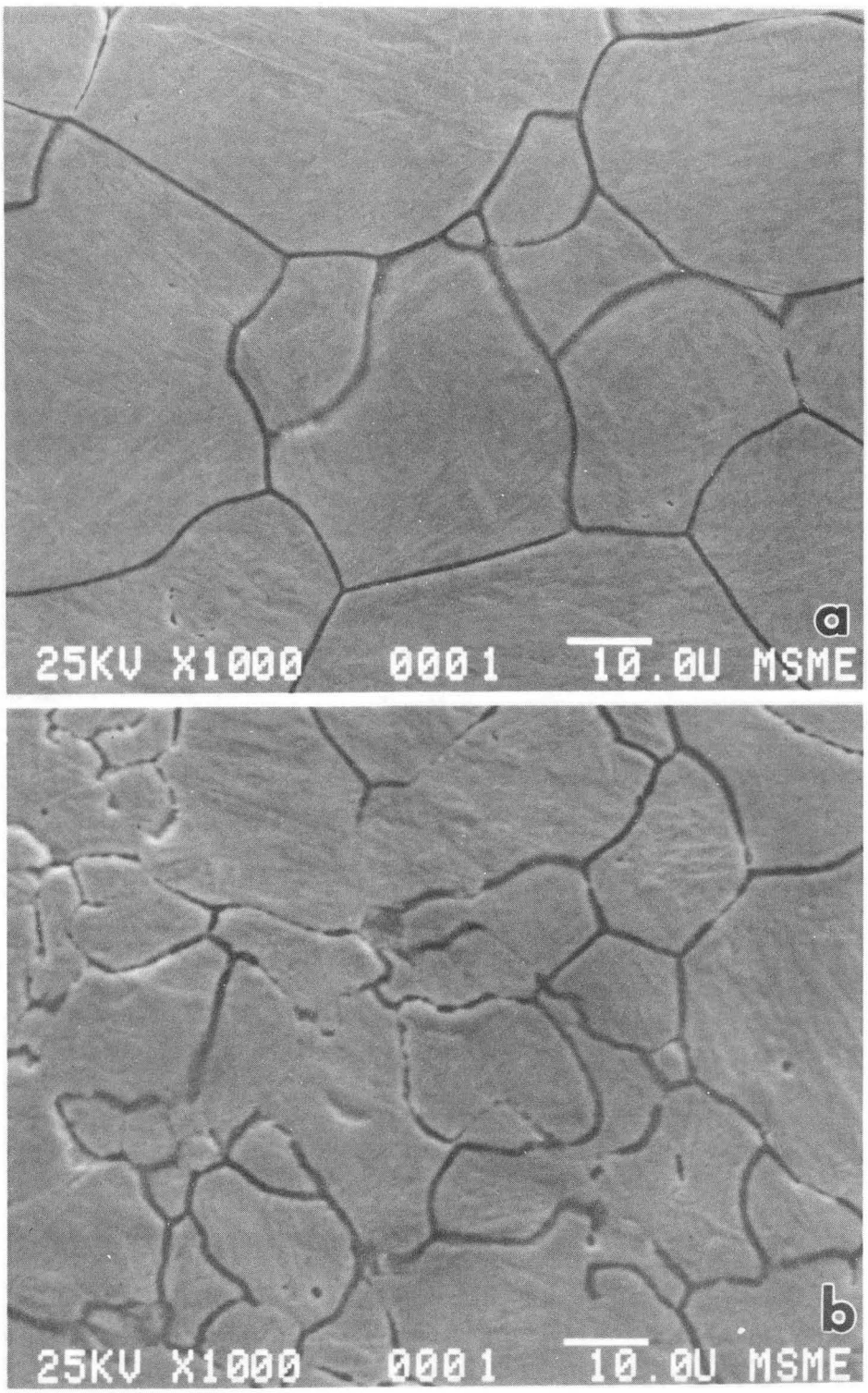

XBB 880-10524 A

Fig. 10

XBB 880-10528 A

Fig. 11

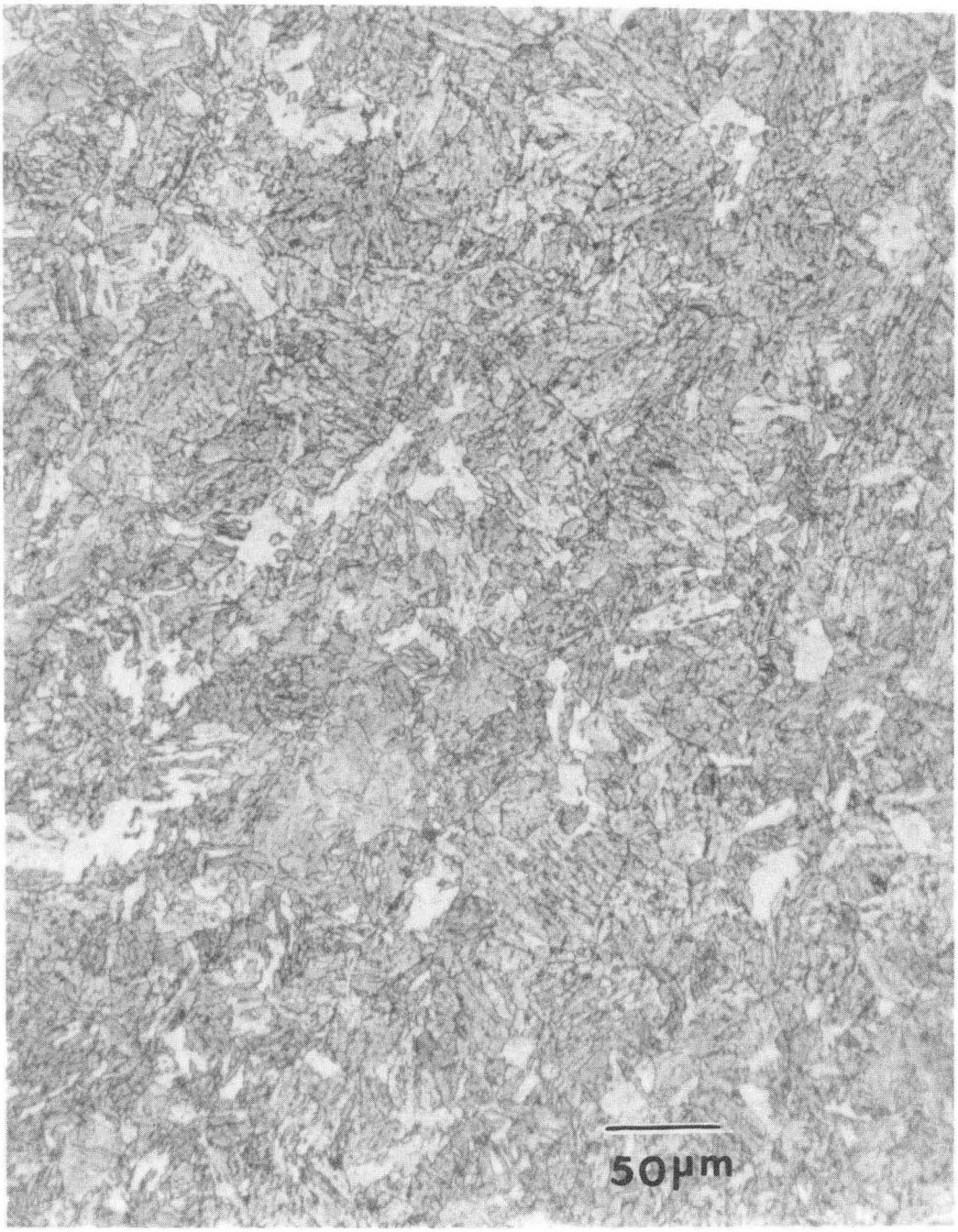

XBB 880-10527 A

Fig. 12

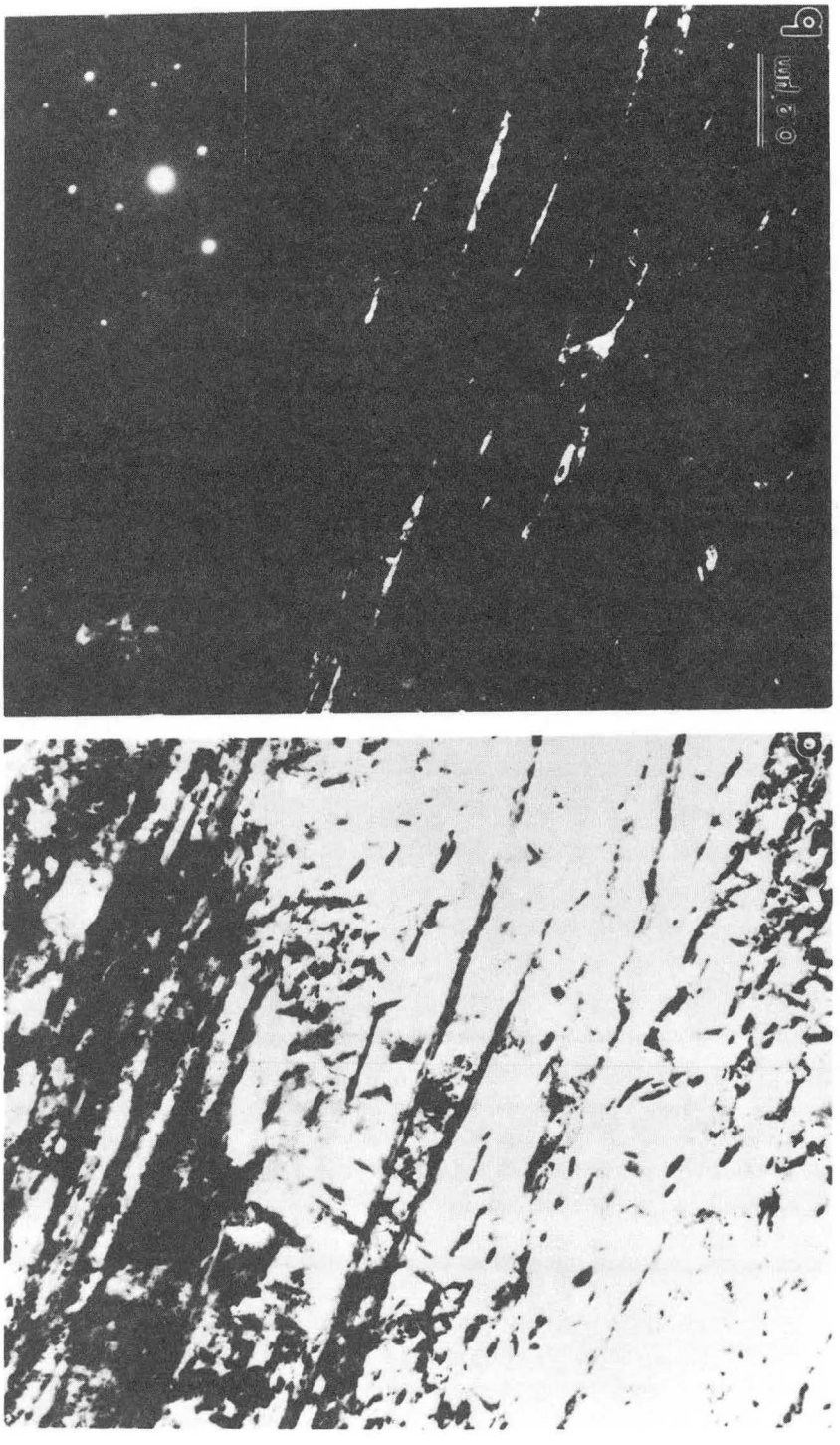

XBB 880-10518 A

Fig. 13

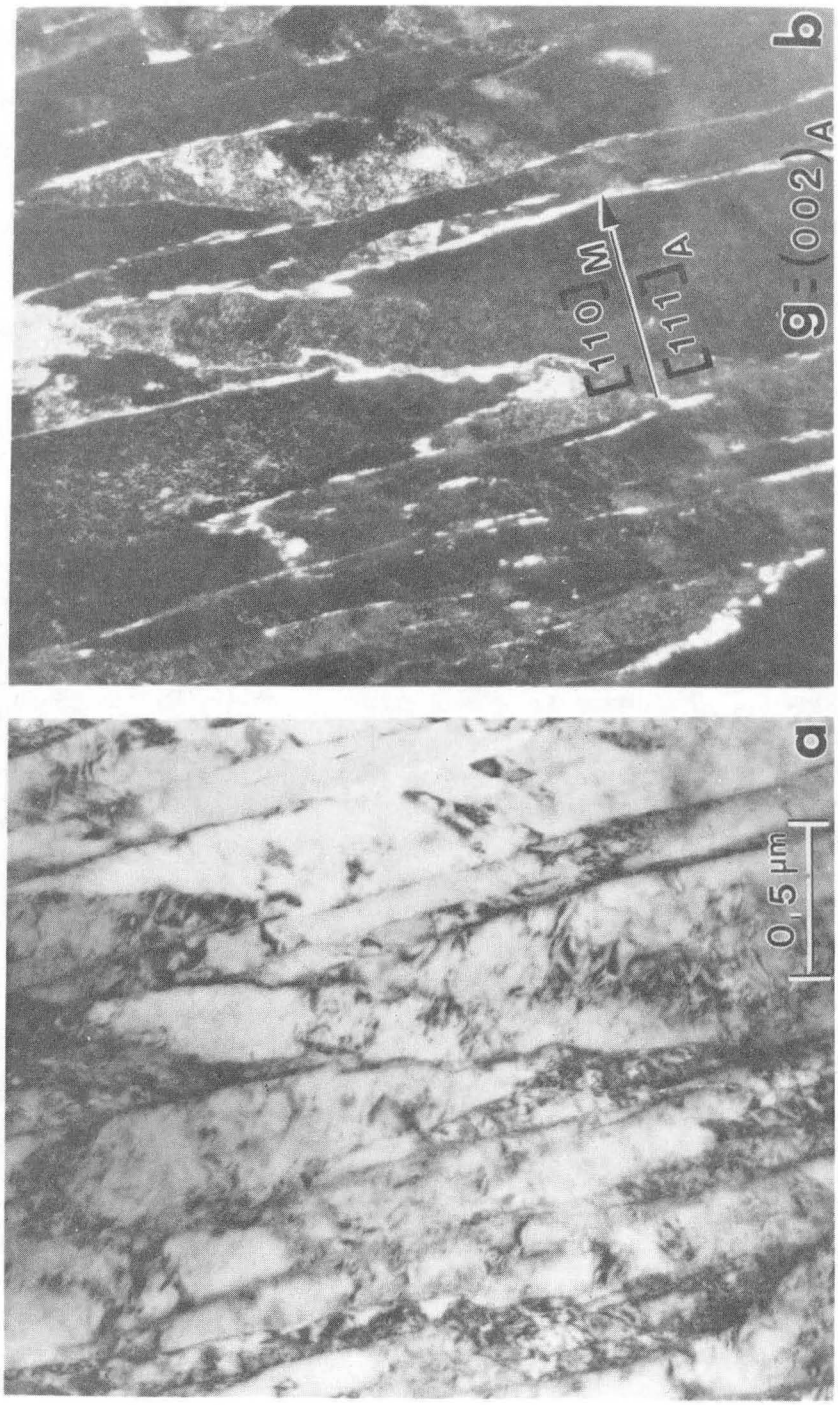

XBB 870-9092 C

Fig. 14

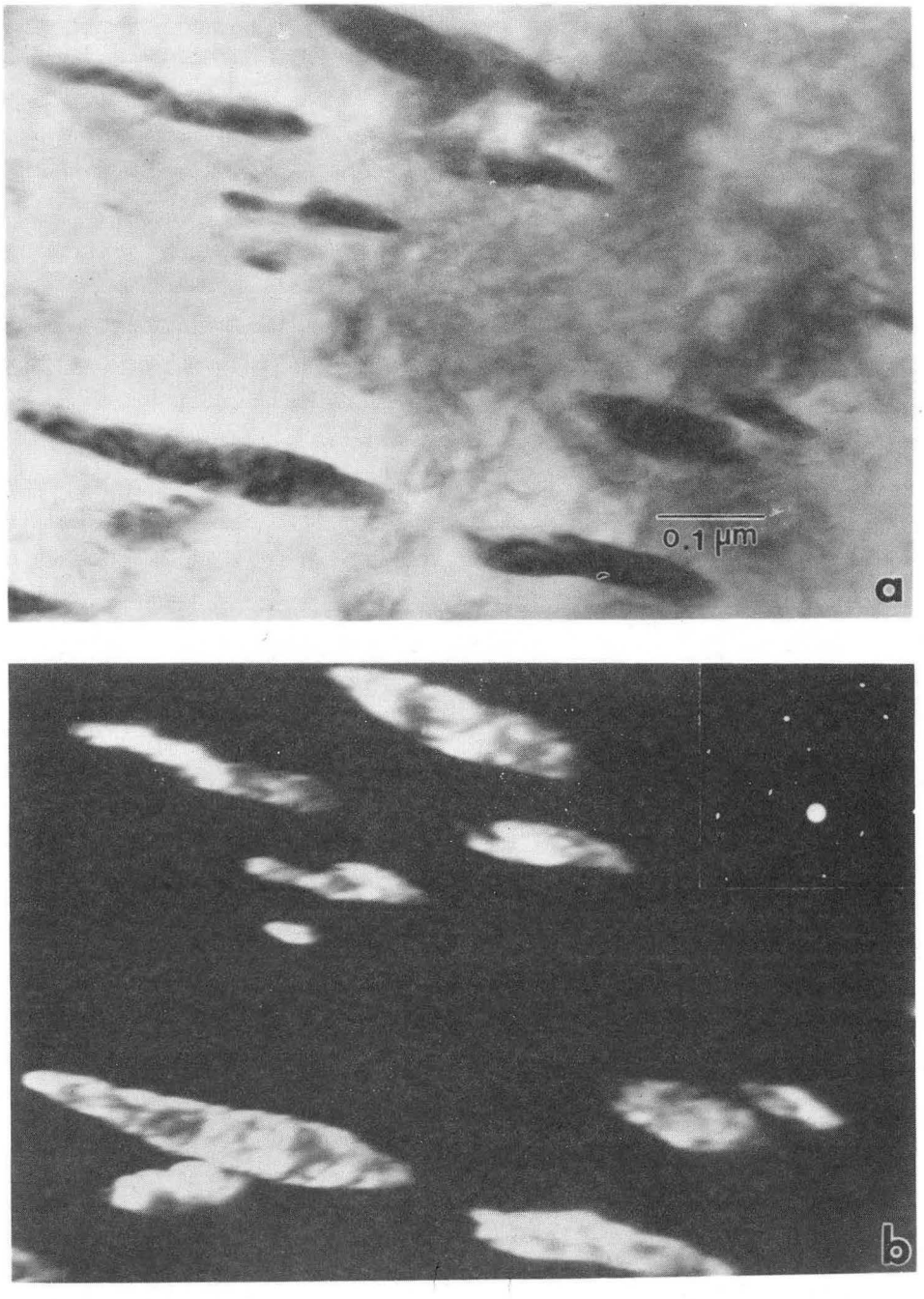

XBB 880-10517 A

Fig. 15

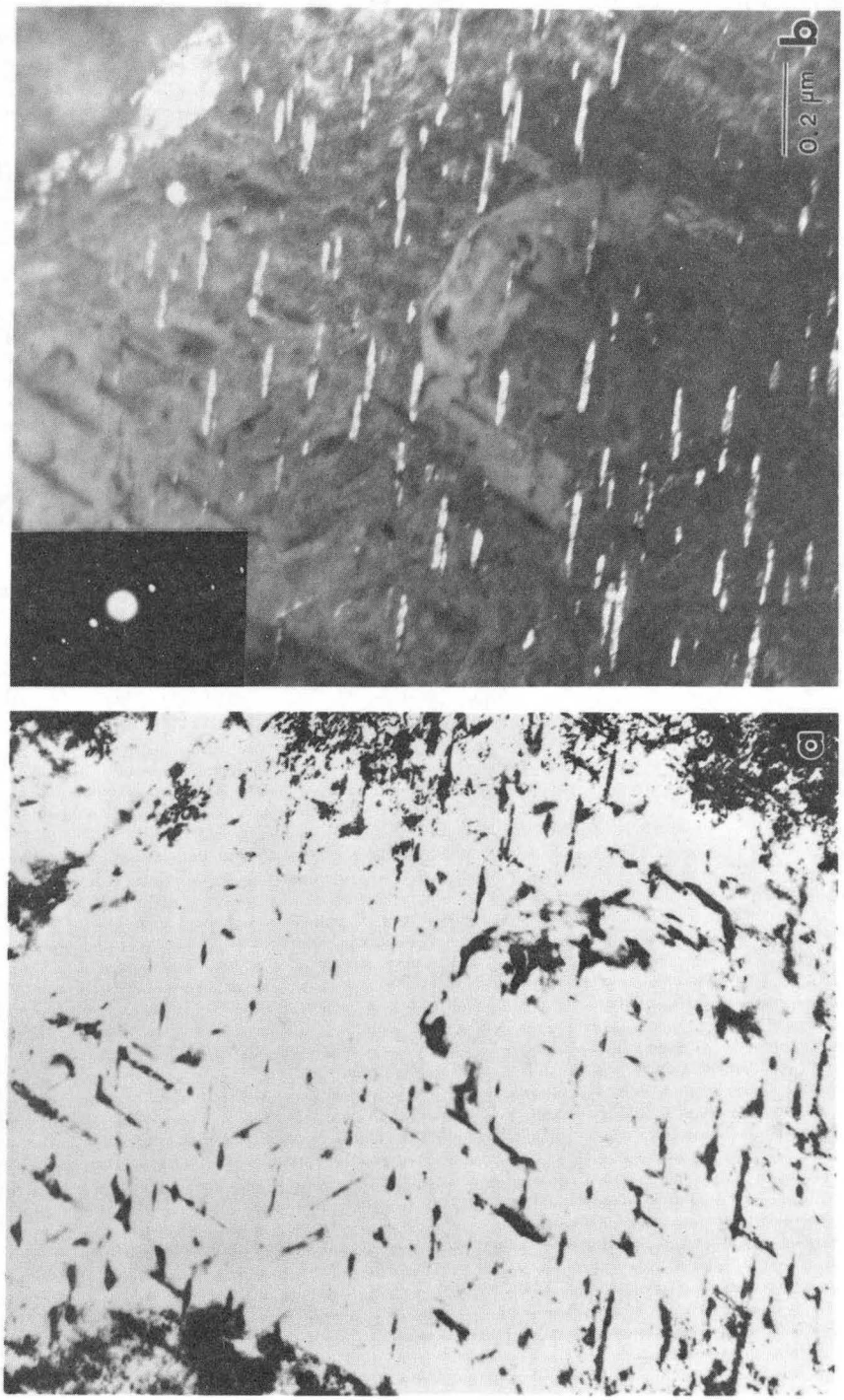

XBB 880-10516 A

Fig. 16

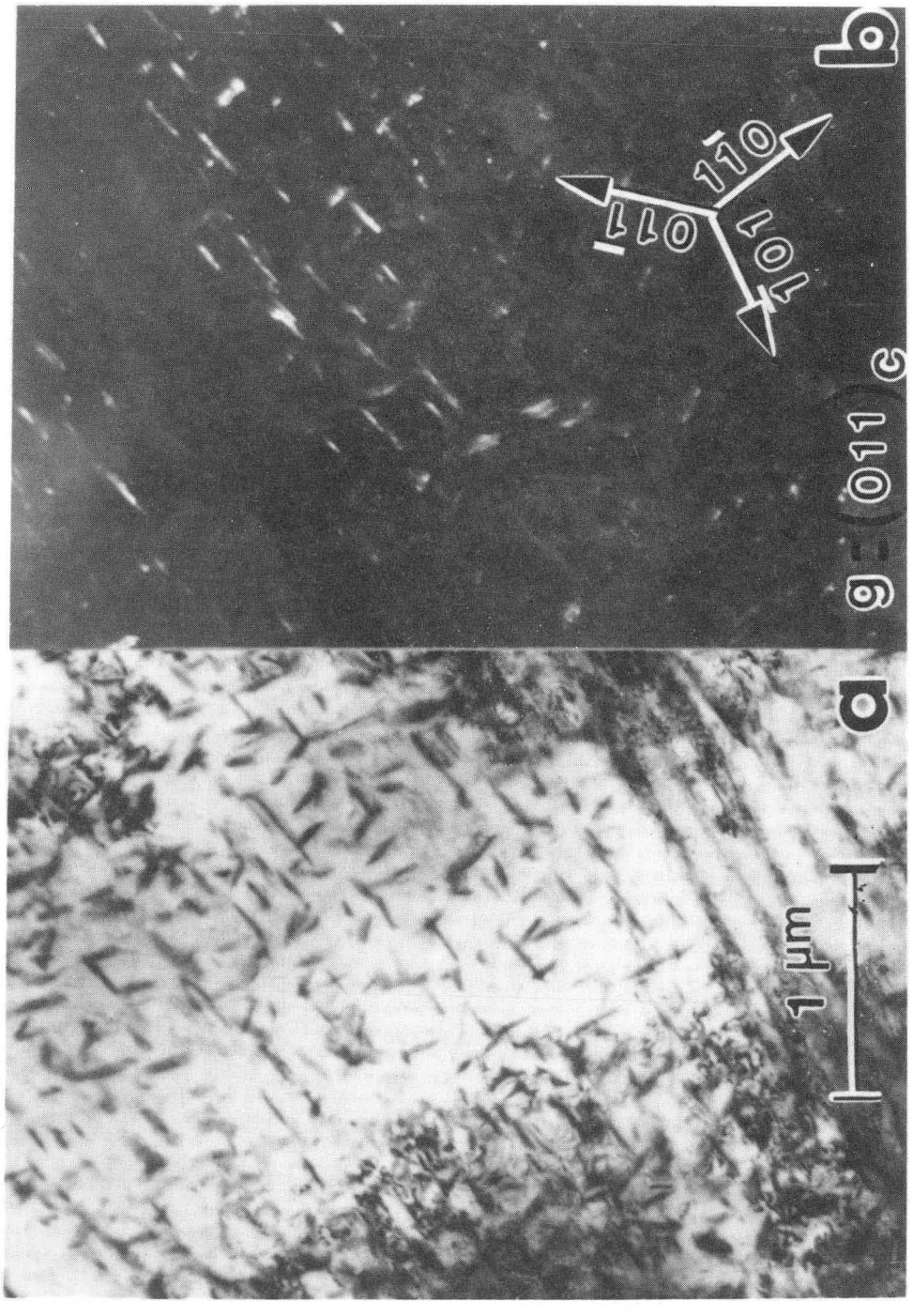

XBB 870-9091 C

Fig. 17

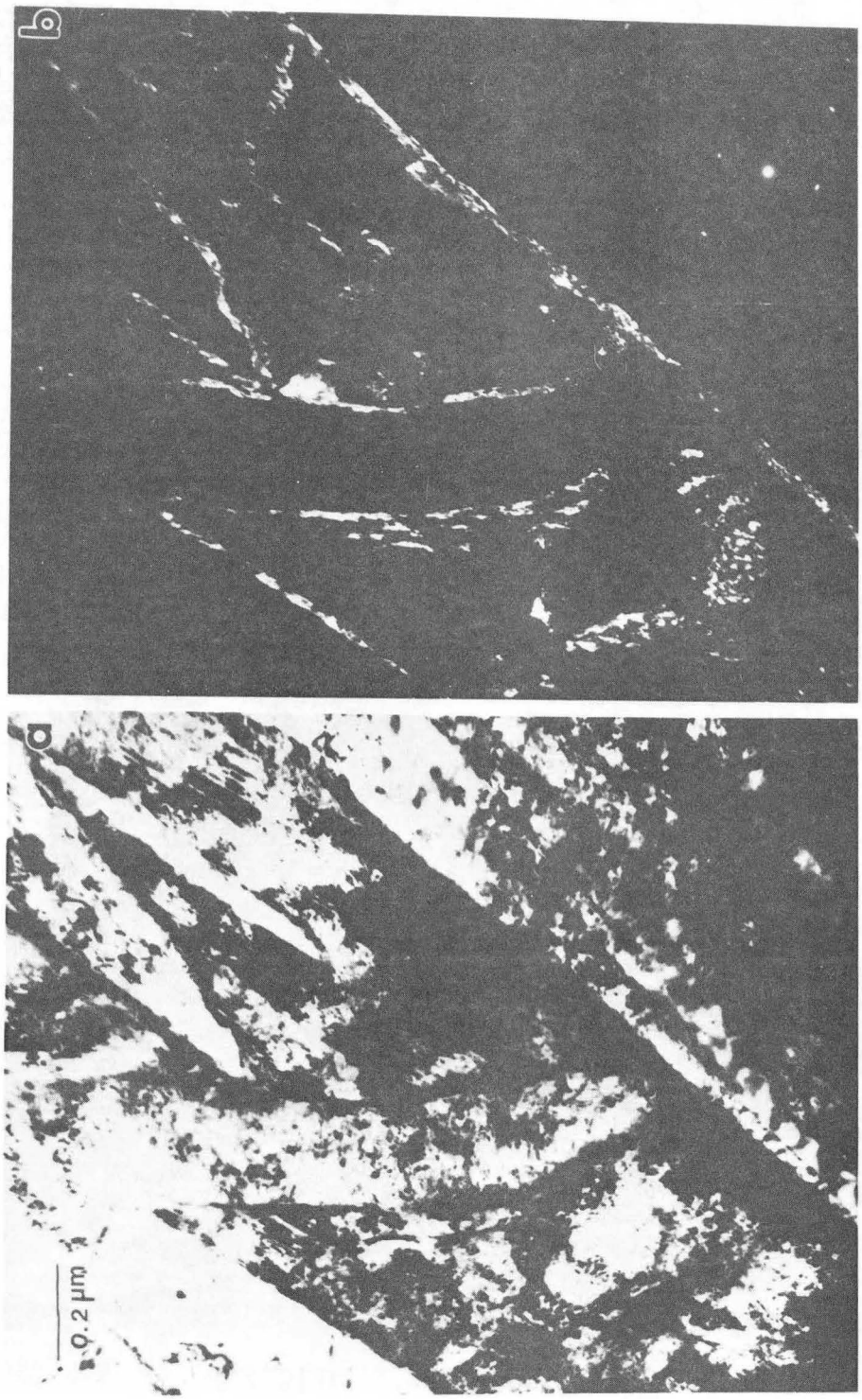

XBB 880-10515A

Fig. 18

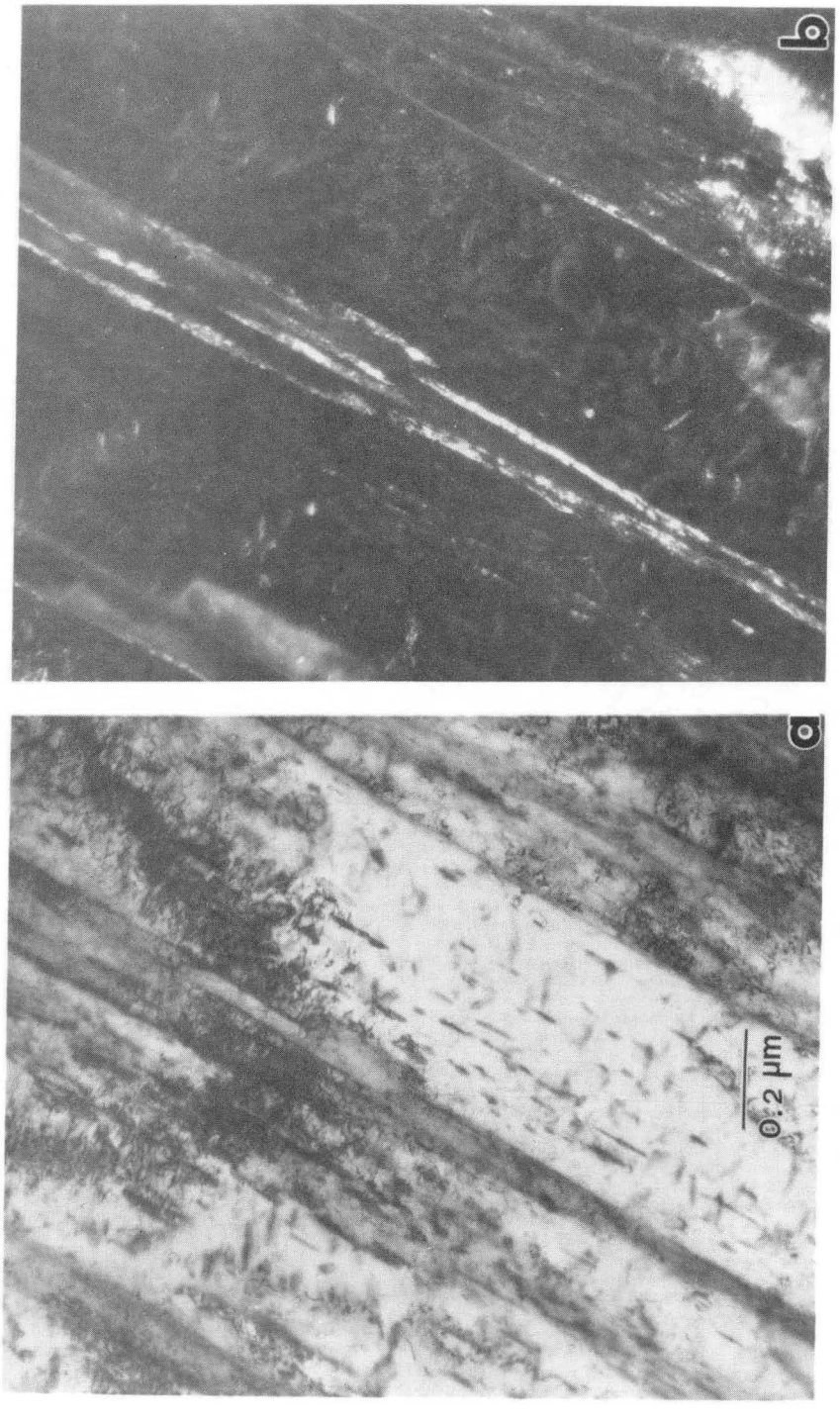

XBB 880-10514 A

Fig. 19

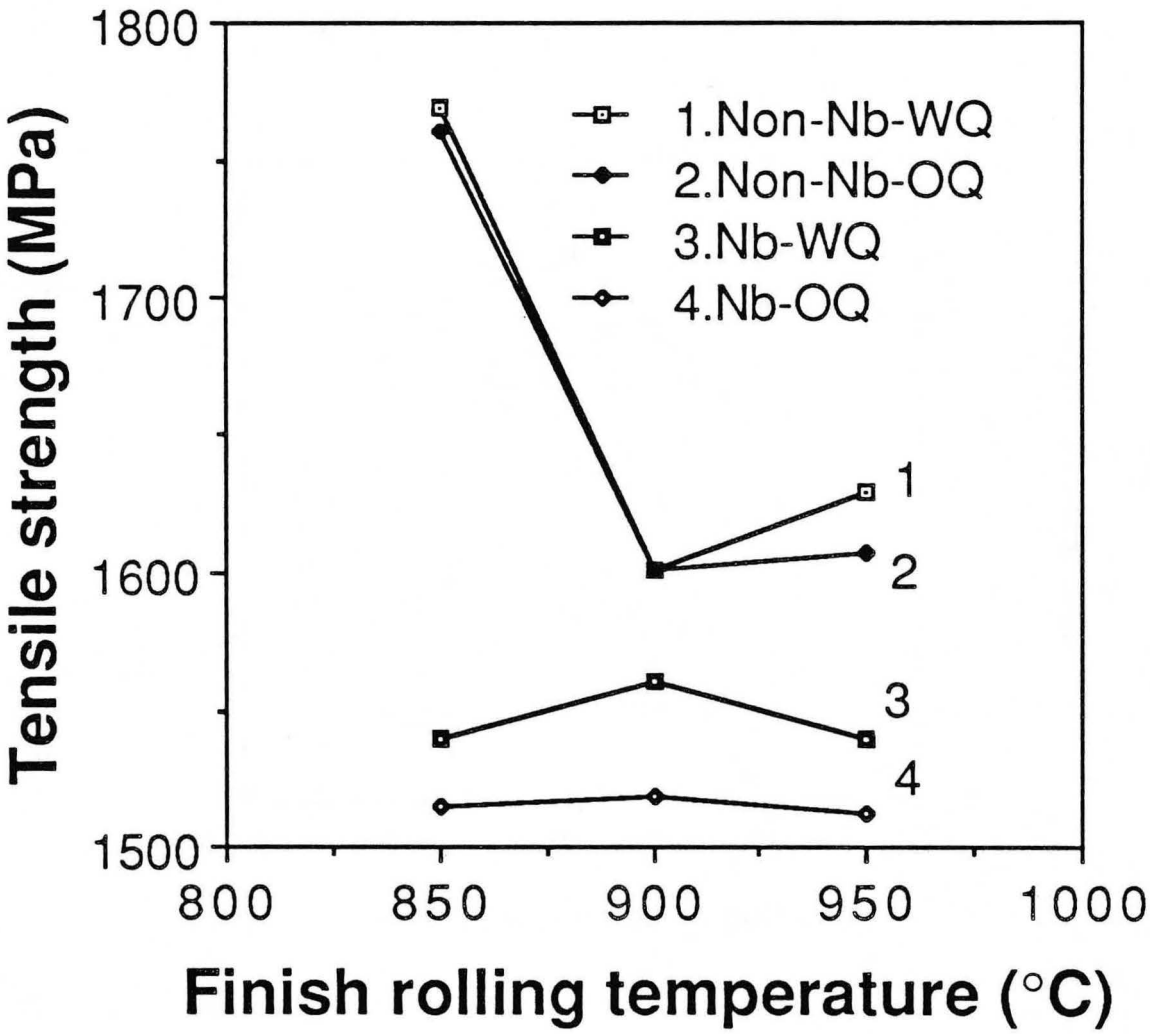

XBL 8811-3778 A

Fig. 20

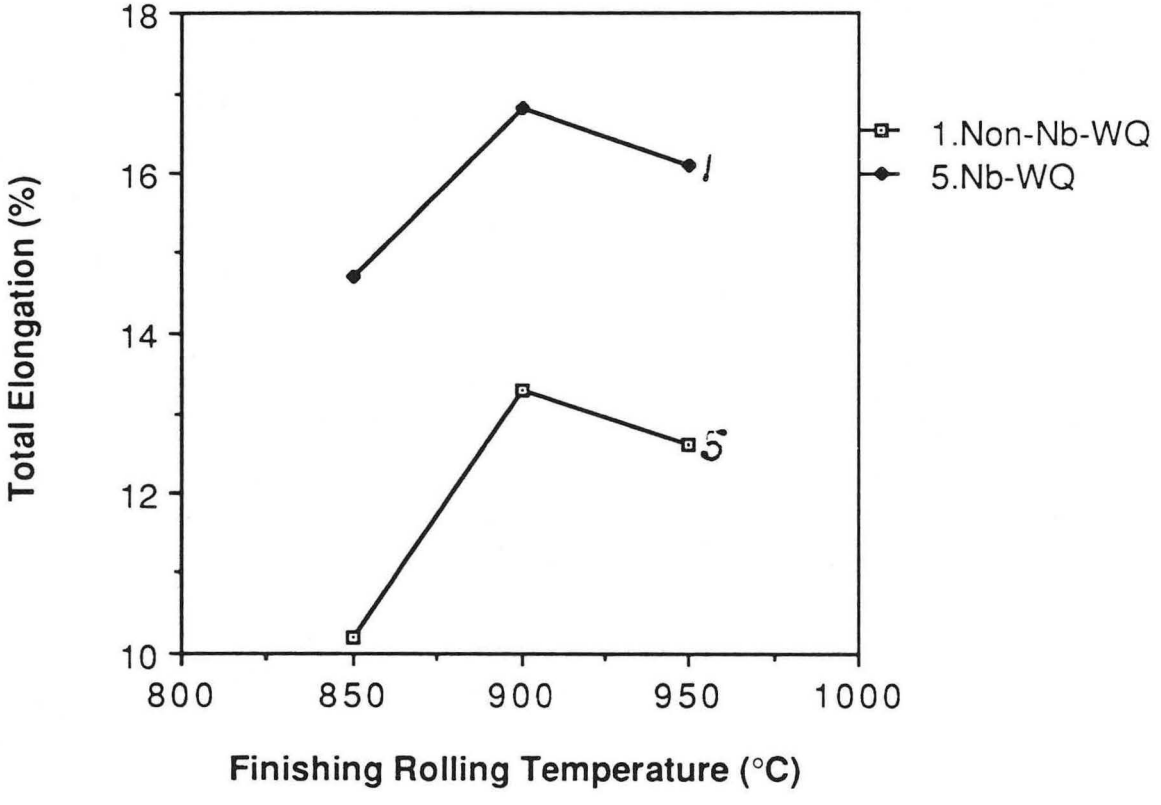

XBL 8811-3779 A

Fig. 21

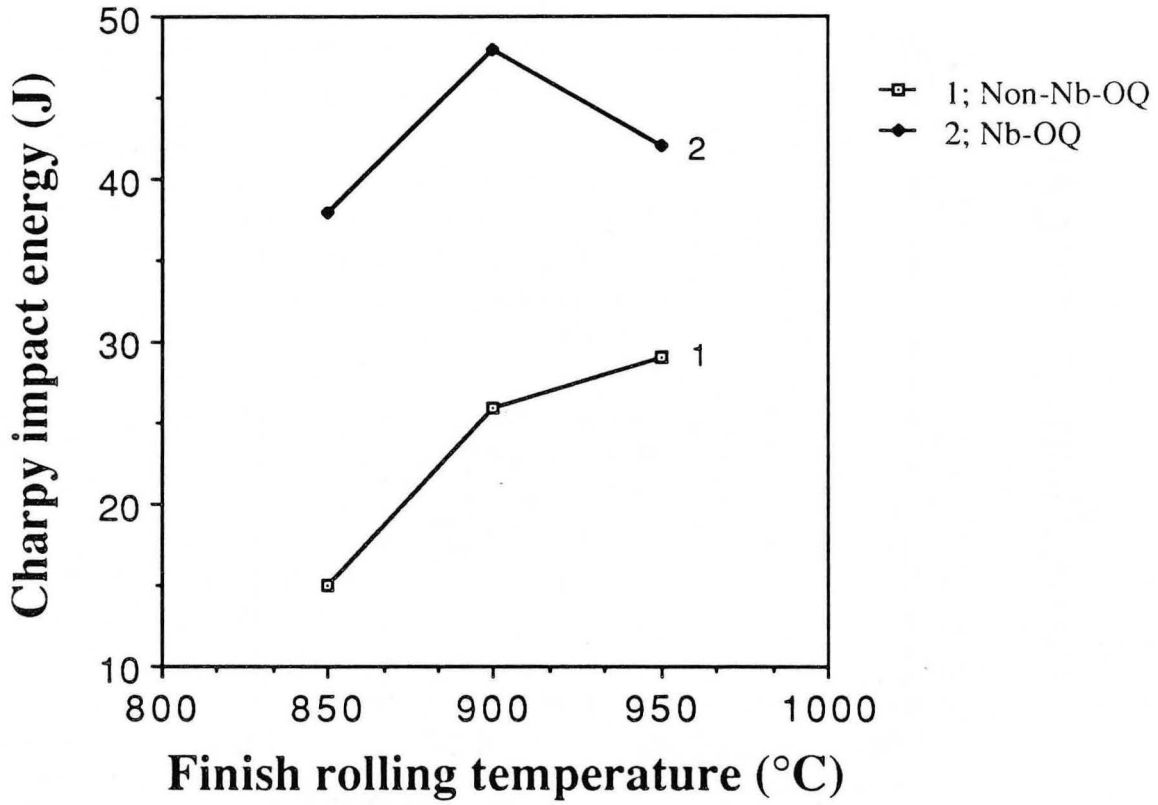
50
40
30
20
10
800
850
900
950
1000
Charpy impact energy (J)
Finish rolling temperature (°C)
1; Non-Nb-OQ
2; Nb-OQ
1
2
XBL 8811-3780 A

Fig. 22

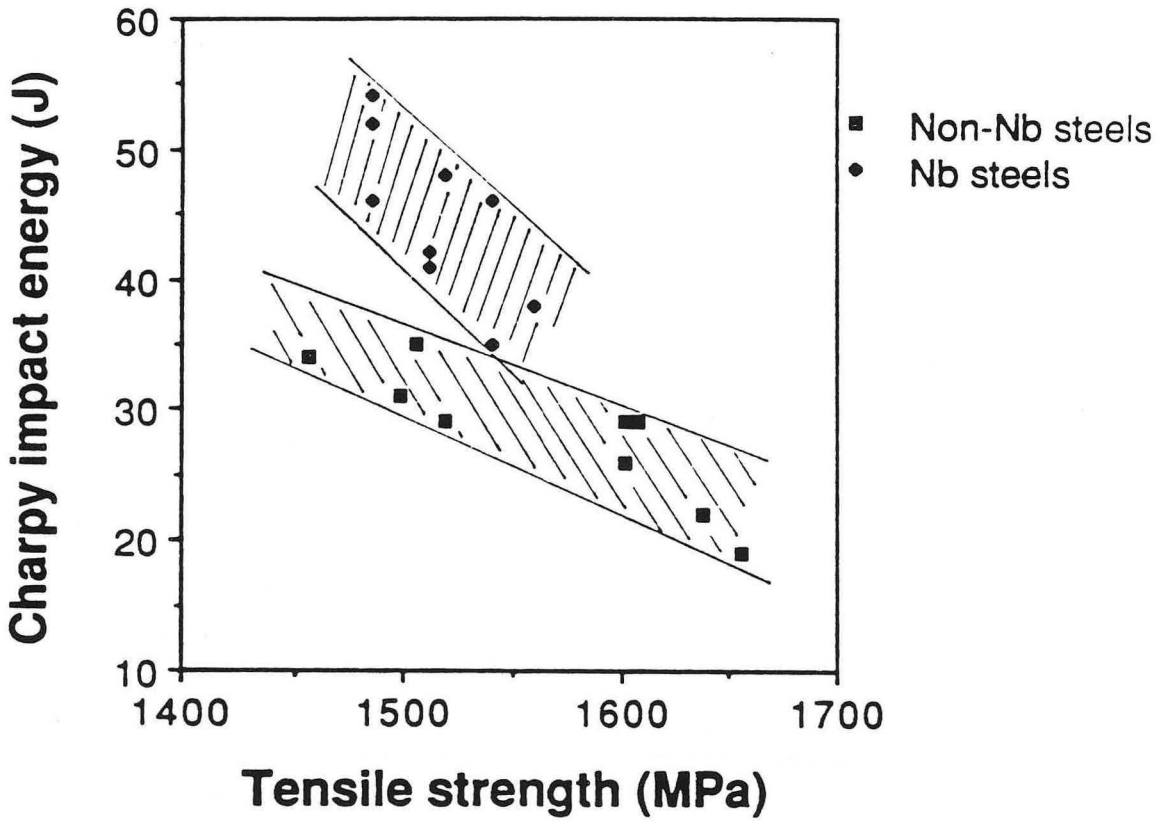

XBL 8811-3781 A

Fig. 23

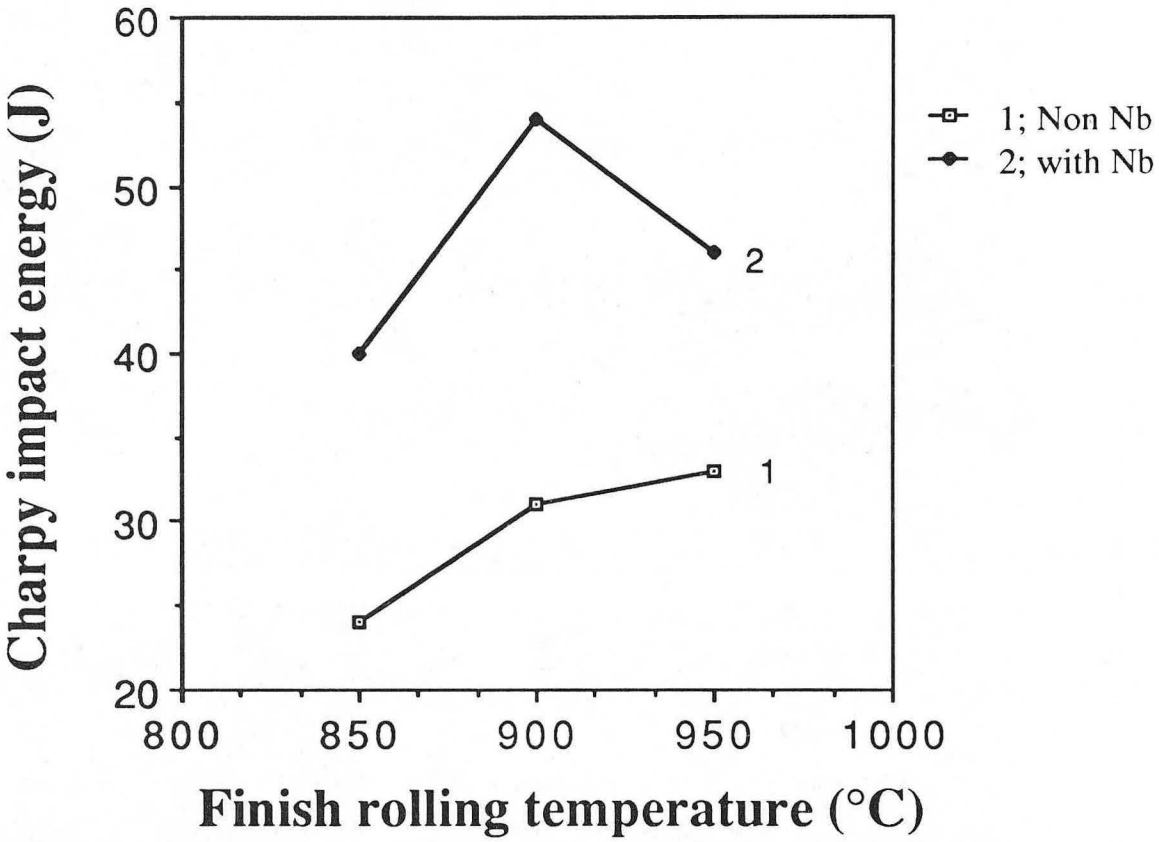

XBL 8811-3782 A

Fig. 24

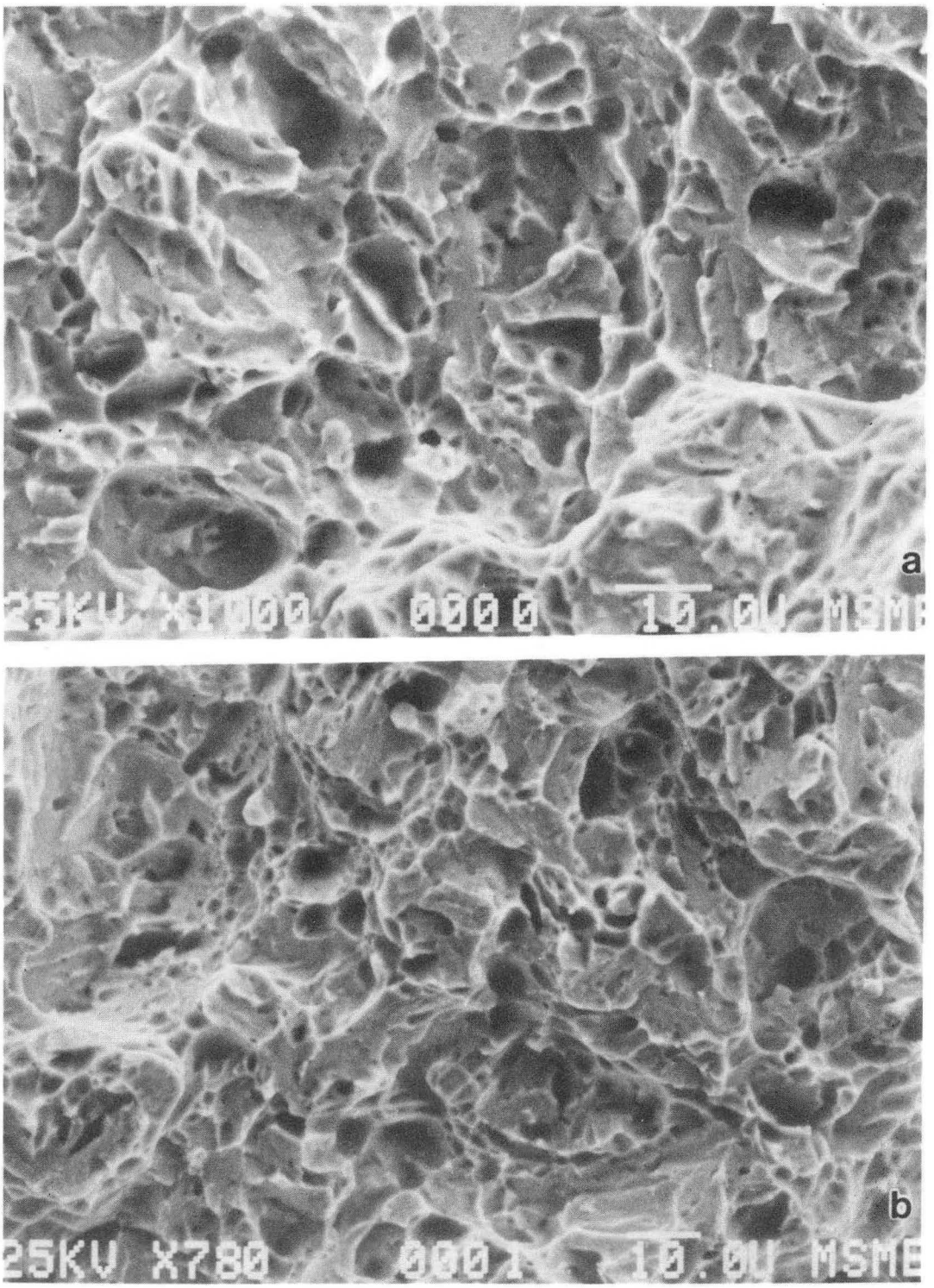

XBB 880-10523 A

Fig. 25

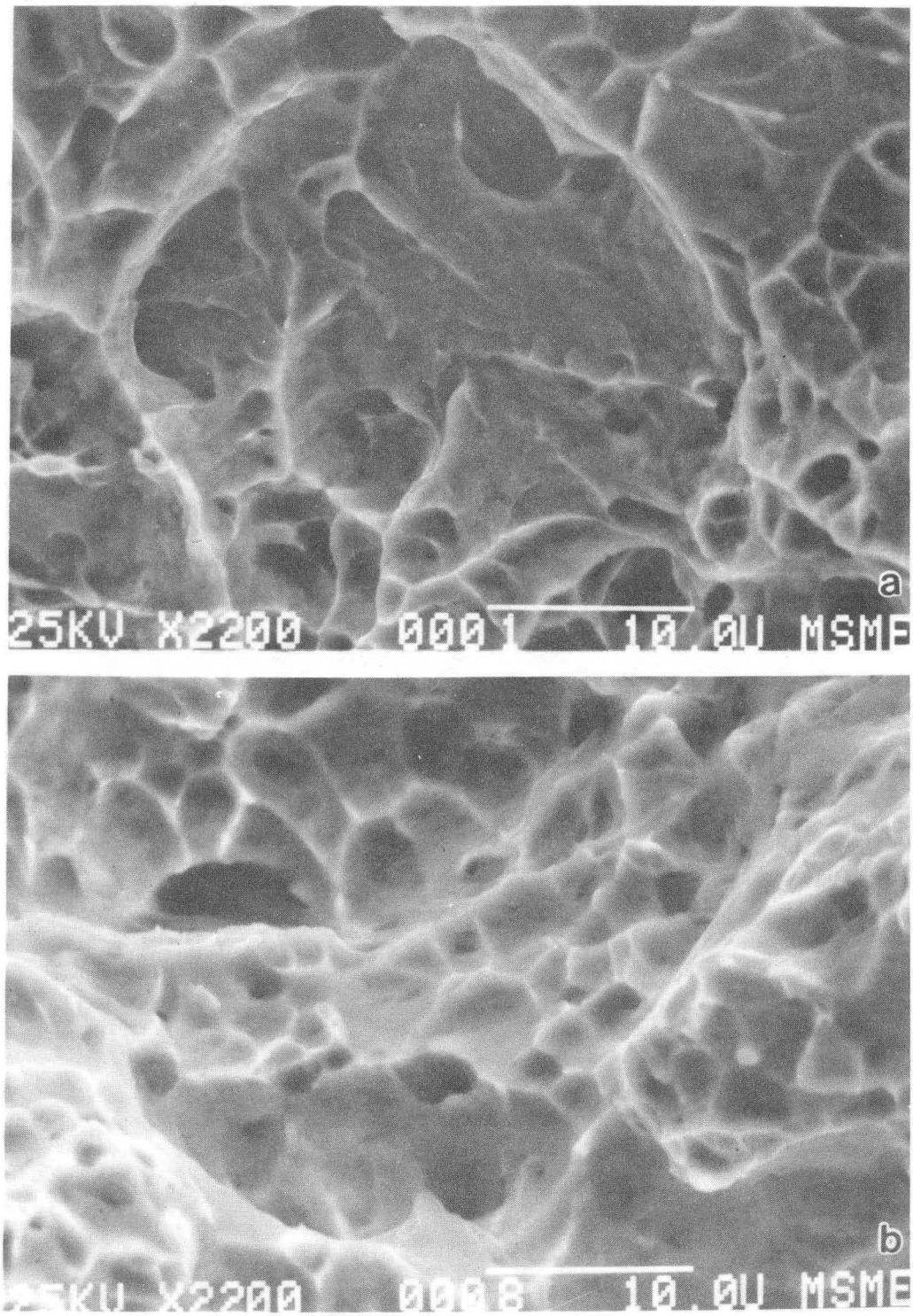

XBB 880-10522 A

Fig. 26

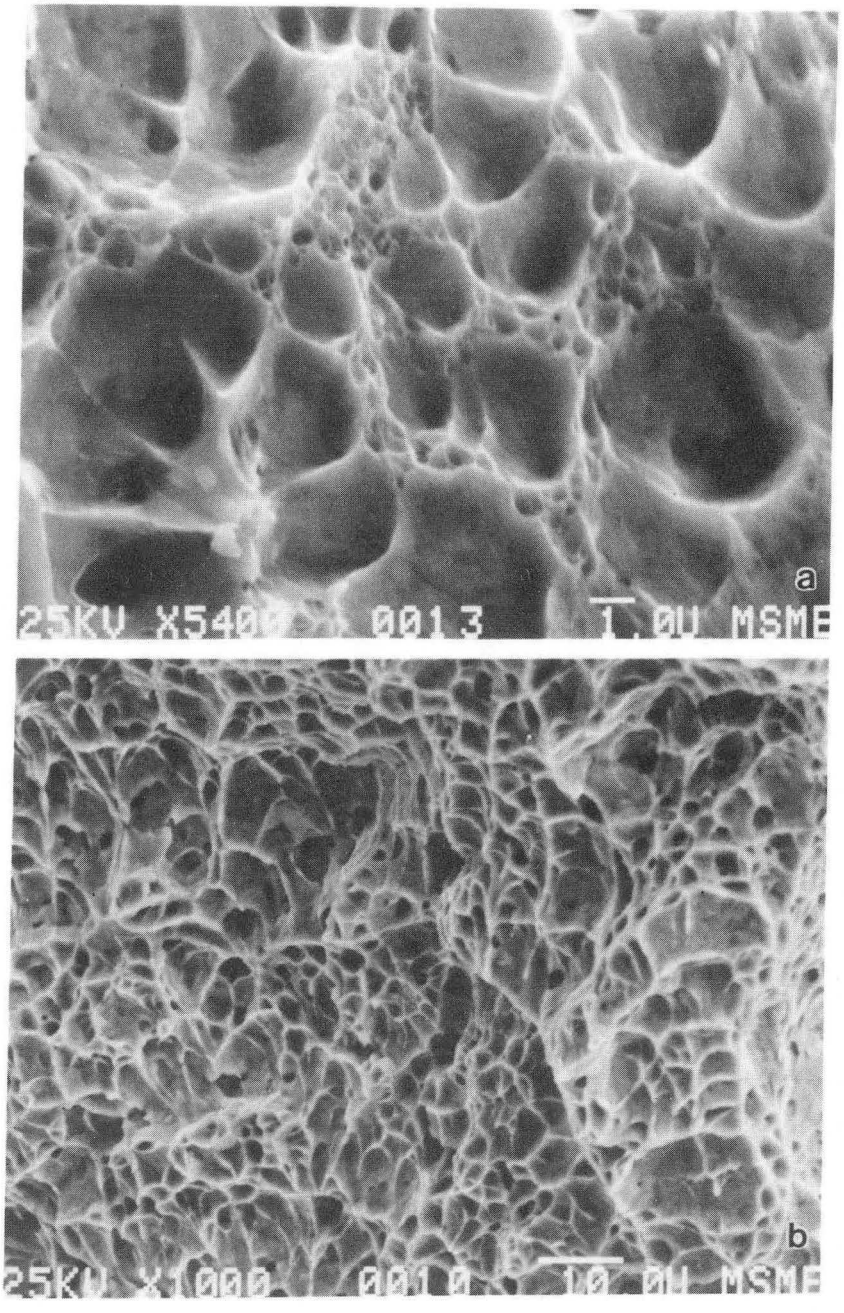

XBB 880-10521 A

Fig. 27

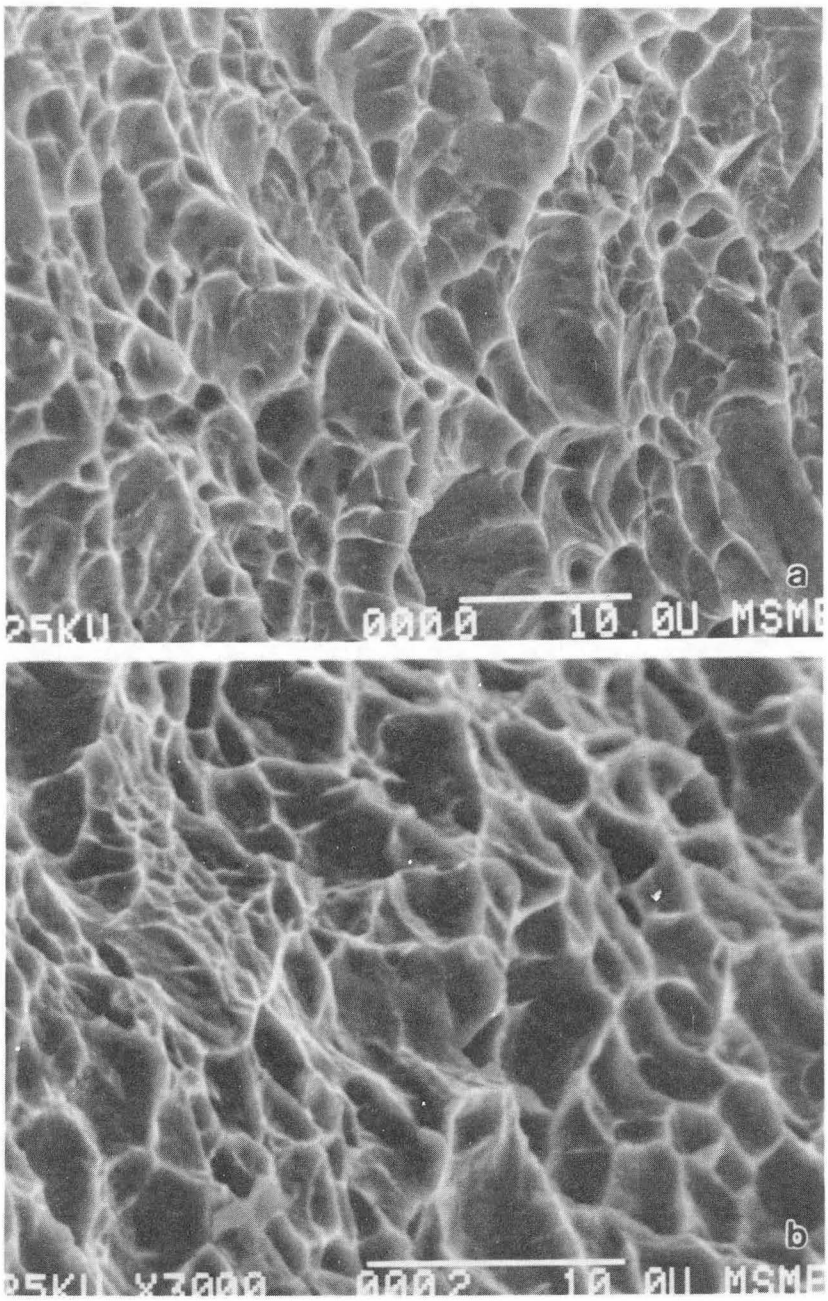

XBB 880-10520 A

Fig. 28

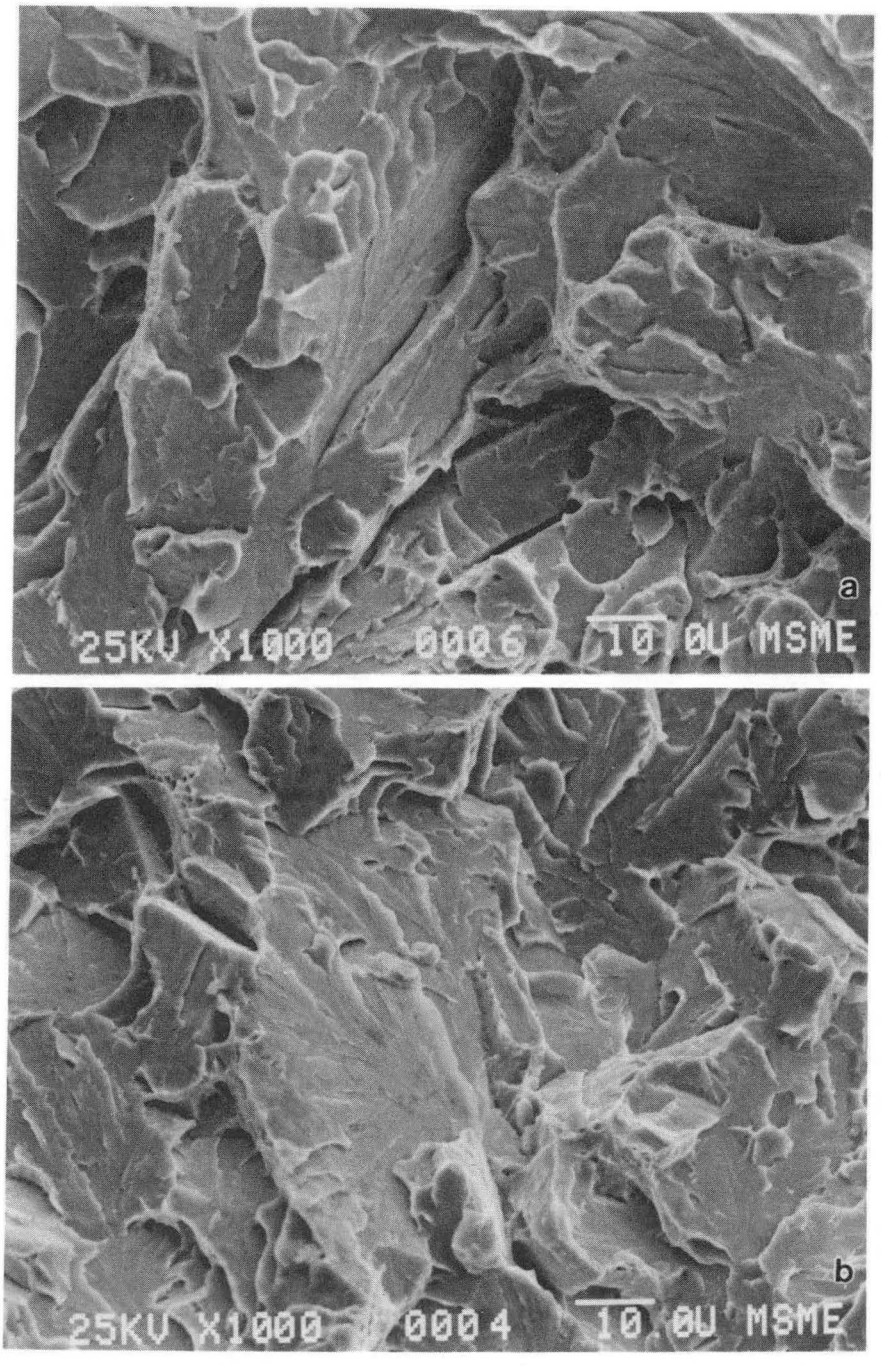

XBB 882-1390 B

Fig. 29

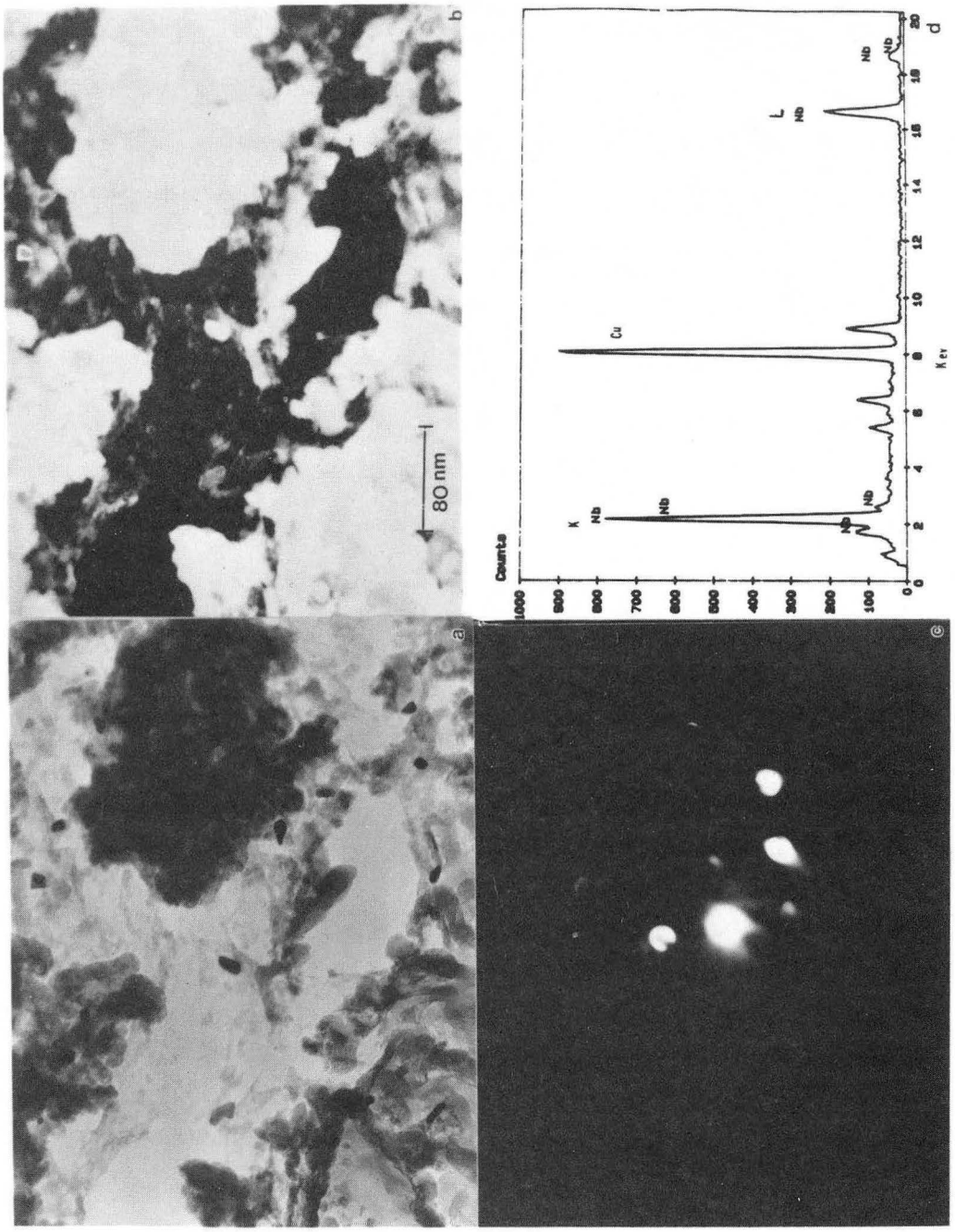

Fig. 30

XBB 880-10519 A

LAWRENCE BERKELEY LABORATORY
TECHNICAL INFORMATION DEPARTMENT
1 CYCLOTRON ROAD
BERKELEY, CALIFORNIA 94720